This is to certify that the

dissertation entitled

ELECTROMAGNETIC INTERACTIONS

IN INTEGRATED ELECTRONIC CIRCUITS

presented by

Michael John Cloud

has been accepted towards fulfillment
of the requirements for

Ph.D. degree in Electrical Engineering

Major professor

Date Sept. 2, 1987

ELECTROMAGNETIC INTERACTIONS

IN INTEGRATED ELECTRONIC CIRCUITS

By

Michael John Cloud

A DISSERTATION

Submitted to
Michigan State University
in partial fulfillment of the requirements
for the degree of

DOCTOR OF PHILOSOPHY

Department of Electrical Engineering and Systems Science

1987

ABSTRACT

ELECTROMAGNETIC INTERACTIONS
IN INTEGRATED ELECTRONIC CIRCUITS

By

Michael John Cloud

Electromagnetic waves in millimeter-wave integrated circuits are studied. Dielectric film and cover regions overlay a conducting half-space in the configuration modeled, forming a nonuniform background for integrated devices. Emphasis is placed upon the microstrip transmission line in this environment.

This research exploits an integral-operator description of the system. Constructed through Hertz potentials, an electric field integral equation (IE) quantifies microstrip surface currents. Complex plane analysis in the axial Fourier transform domain leads to the rigorous identification of discrete and continuous eigenvalue spectra. Discrete modes are associated with simple pole singularities, while the continuous spectrum arises from branch-cut integrals. These modal spectra are subsequently linked to natural and forced solutions of the IE.

Discrete wave modes are associated with the homogeneous IE, which is solved by the moment method for electrically-thin microstrip. The current density function is expanded in both subsectional and entire-domain basis functions. Results clearly validate: (1) the dominant axial current approximation for narrow strips, and (2) the edge

singularity for axial currents. Dispersion characteristics are given for several modes; those for the fundamental mode compare favorably with results already in the literature.

Solution of the forced IE, at points along the complex-plane branch cut, yields spectral components of strip radiation modes. The forcing function is taken to be the electric field impressed by a vertical monopole current that resides in the film layer. Preliminary moment-method results are given.

The transform-domain IE is also a basis for the study of coupling phenomena in axially-uniform multi-strip systems. System propagation modes are characterized by coupled currents sharing simple-pole singularities. Perturbation approximations apply for loose coupling, leading to an overlap-integral description of the coupling phenomenon.

Finally, a novel approach to the numerical evaluation of Sommerfeld integrals, using the Fast Fourier Transform, is advanced.

ACKNOWLEDGMENTS

The author is grateful to major professor Dennis P. Nyquist and co-thesis advisor Byron C. Drachman for their guidance throughout this research. In addition, he wishes to thank guidance committee members K.M. Chen and E.J. Rothwell for their encouragement and support.

Funding for the project was provided by the Office of Naval Research, grant # N0014-86-K-0609.

TABLE OF CONTENTS

LIST OF FIGURES

CHAPTER I

INTRODUCTION

The subject of high-frequency, planar integrated circuits is becoming increasingly important. Rapid evolution in this technology suggests a need for new, more rigorous methods of analysis.

This dissertation addresses the media configuration indicated in Figure 1. A dielectric film layer resides between two other regions: perfectly conducting ground plane, and dielectric cover. Conducting devices (e.g., microstrip lines [1], patch antennas [2]) are integrated over the film/cover interface. High-speed integrated electronic circuits operating at microwave and millimeter wave frequencies use microstrip connections. The strip is an attractive transmission line for applications requiring high packaging densities [3].

Commonly, the analysis of circuit performance proceeds through a combination of low-frequency electric circuit and quasi-TEM transmission line theories. These are only approximate at high frequencies and circuit densities. In modern configurations electromagnetic phenomena play key roles in terms of both losses and coupling between adjacent integrated devices.

Except for an integral equation analysis by Wu [4] of the principal propagation mode, the isolated microstrip line is studied primarily via the quasi-TEM electrostatic approximation. Existing quasi-TEM formulations are typified by the variational method of [5].

Microstrip open-end and gap discontinuities are examined by full-wave analysis in [6]. The finite microstrip segment finds many applications as a radiating element; this problem is treated, for example, in [7,8,9,10].

This research exploits a conceptually exact integral-operator description of the integrated circuit, with primary emphasis on the microstrip transmission line. The seven chapters of this dissertation treat various parts of the microstrip problem. The goal of Chapter 2 is to develop and emphasize certain parts of the relevant EM theory. Chapter 3 formulates an electric field integral equation, which is the basis for all subsequent work; later in Chapter 3, Fourier transform and complex plane analyses quantify the proper microstrip eigenmode spectrum. Discrete modal surface currents are detailed in Chapter 4. Chapter 5 treats the continuous spectrum. Finally, a simple coupled-mode theory for parallel microstrips is advanced in Chapter 6.

Some words about notation here might be helpful. All integrals, unless limits are explicitly shown, are over the entire real line. As is standard in most electrical engineering works, the symbol j denotes the elementary imaginary number. Vector quantities are embellished with arrows, and are also slightly boldfaced for emphasis. Dyadic quantities (also slightly boldfaced) appear with a double overbar. Finally, a simple-harmonic time dependence is assumed, but supressed, throughout the dissertation.

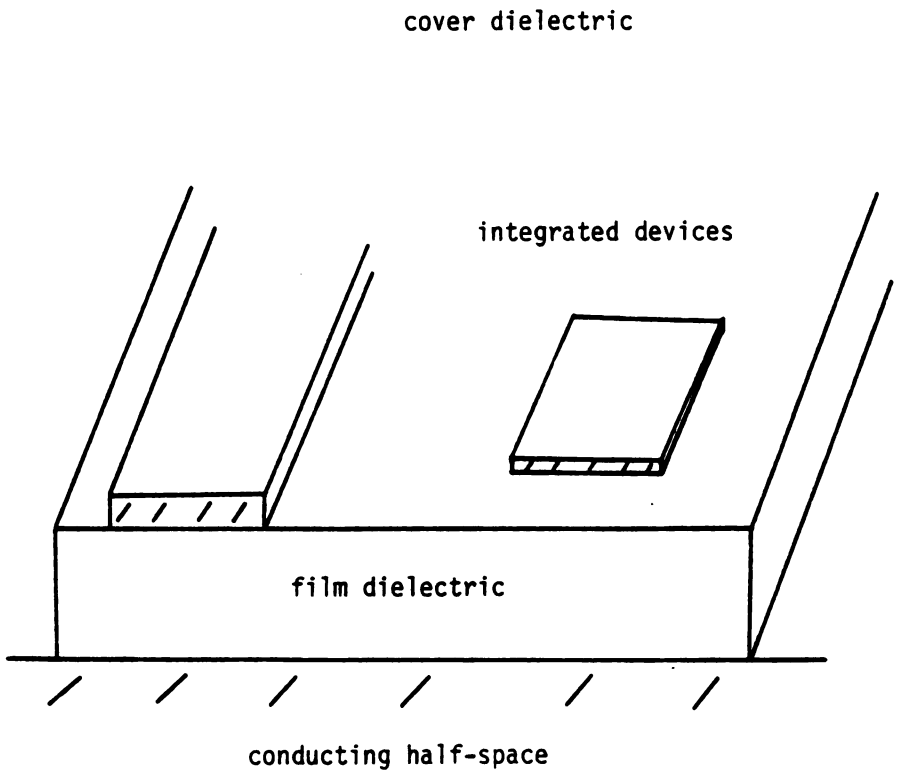

Figure 1. Basic form of high-speed integrated circuit.

CHAPTER II

BASIC EM FORMULATION FOR INTEGRATED ELECTRONICS

2.1 Introduction and Geometry

The electromagnetic description of integrated electronics embraces the theory of EM waves in layered dielectric media. An integral operator method is required here, because boundary conditions of differential-operator methods are inseparable for many device geometries [11]. Integral-operator formulations are also well-adapted to techniques of numerical solution. Hertz potentials, expressed as Fourier integrals, are employed in the present analysis; the challenge faced in this chapter is to derive practical boundary conditions for their components.

Consider the setting displayed in Figure 2. A perfectly conducting half-space is overlayed with a dielectric film having refractive index n_f and thickness t; the film is, in turn, covered by a dielectric having refractive index n_c. All materials are assumed nonmagnetic and infinite in extent.

For a suitable geometry, choose a rectangular coordinate system with z-axis parallel to the microstrip waveguiding axis; x and y axes are tangent and normal, respectively, to the cover/film interface. Define unit vector $\hat{t}$ as locally tangent to all conducting device surfaces. See Figure 2.

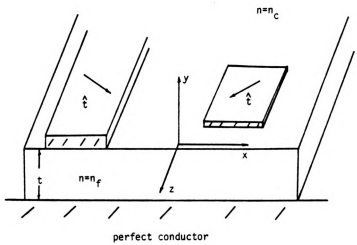

Figure 2. Geometry and medium parameters.

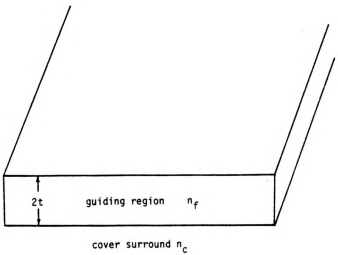

Figure 3. Symmetric slab dielectric waveguide.

2.2 Symmetric-slab Interpretation

The cover/film/conductor complex constitutes the background environment of an integrated device such as the microstrip line. It is appropriate to think of this layered-media background structure's behavior as a symmetric-slab dielectric waveguide. Classical image theory implies a guiding region dielectric having thickness 2t, of course, because all phenomena have mirror images through the plane at y=-t. Some interpretations in subsequent chapters are based upon this idea; therefore, a brief summary and discussion of the symmetric-slab guide is given in the next section.

2.3 Homogeneous Dielectric Slab Guide

Assuming axial dependence of electromagnetic fields as $\exp(-j\beta z)$, where β is a phase constant, a transverse-longitudinal decomposition of Maxwell's equations is achieved in standard guided-wave theory [12]. Longitudinal ($\hat{z}$-directed) field components satisfy resulting two-dimensional Helmholtz equations, and serve as generating functions for transverse field components. This formulation, applied to the symmetric slab guide of Figure 3, gives the well-known slab field distributions.

Quasi-standard symmetric-slab terminology exists. The guide is composed of a guiding region embedded in an unbounded dielectric cover surround (see Figure 3). Transverse-electric (TE) and transverse-magnetic (TM) modes are identified for which the z-component of electric and magnetic fields, respectively, are zero. Surface waves are discrete, guided-wave modes propagating axially and decaying exponentially in the y-direction; these modes exhibit no transverse

(y directed) power flow. Distinguished by oscillatory, standing-wave solutions in the guiding region, surface waves arise physically from total internal reflection when $n_f > n_c$. It is conventional to further classify them as even or odd in their transverse field components. Radiation modes are spectral-component fields exhibiting oscillations in both guiding region and surround; such modes do allow transverse power flow into the surround.

Phase constant β for a surface-wave mode is restricted to the existence interval (k_c, k), where k and k_c are the guiding region and surround wavenumbers. For radiation-modes, β^2 is confined to be less than k_c^2. These results follow directly from the mode type definitions.

The fundamental surface-wave mode is the TM_0, an even mode with no low-frequency cutoff regardless of guiding region thickness. Its characteristic equation is

$$\tan(Kt) = n^2\gamma/n_c^2K \tag{2.1}$$

where n and n_c are guiding region and surround refractive indices, and K and γ are the guiding region and surround eigenvalues defined by $K^2=n^2k_o^2-\beta^2$ and $\gamma^2=\beta^2-n_c^2k_o^2$.

2.4 Hertz Potential Representation for EM Fields

Electric and magnetic fields are obtained through the electric-type Hertz [13] potential $\vec{Z}$ (notation following [14]) as

$$\vec{E} = k^2\vec{Z} + \nabla\nabla\cdot\vec{Z} \tag{2.2a}$$

$$\vec{H} = j\omega\varepsilon\nabla\times\vec{Z} \tag{2.2b}$$

The Hertz potential satisfies an inhomogeneous vector Helmholtz equation with source term $-\vec{J}/j\omega\varepsilon$; this term represents time-harmonic equivalent polarization sources. Expanded in rectangular components, the electric and magnetic field intensities are

$$E_x = k^2 Z_x + (\partial/\partial x)\nabla\cdot\vec{Z} \tag{2.3a}$$

$$E_y = k^2 Z_y + (\partial/\partial y)\nabla\cdot\vec{Z} \tag{2.3b}$$

$$E_z = k^2 Z_z + (\partial/\partial z)\nabla\cdot\vec{Z} \tag{2.3c}$$

$$H_x = j\omega\varepsilon[(\partial/\partial y)Z_z - (\partial/\partial z)Z_y] \tag{2.4a}$$

$$H_y = j\omega\varepsilon[(\partial/\partial z)Z_x - (\partial/\partial x)Z_z] \tag{2.4b}$$

$$H_z = j\omega\varepsilon[(\partial/\partial x)Z_y - (\partial/\partial y)Z_x] \tag{2.4c}$$

These expressions are used in section 2.5 to obtain boundary conditions for components of Hertz potential.

2.5 Boundary Conditions for Hertz Potential

Consider the EM field produced by time-harmonic current sources embedded in the cover medium. Fields in the film and cover regions are linked by boundary conditions applicable at y=0. Boundary

conditions for Hertz potential are consequences of familiar conditions on tangential components of electric and magnetic intensities: at the film/cover interface $E_{cx}=E_{fx}$, $E_{cz}=E_{fz}$, $H_{cx}=H_{fx}$ and $H_{cz}=H_{fz}$; at the film/conductor interface $E_{fx}=0$ and $E_{fz}=0$. Development of Hertz potential boundary conditions proceeds one interface at a time, beginning with the film/cover.

2.5.1 Conditions at Film/Cover Interface

Consider the y=0 interface. Enforcing continuity of tangential electric and magnetic fields in terms of equations (2.3) and (2.4), with definition of the refractive index ratio $N_{fc}=(n_f/n_c)^2$, results in

$$k_c^2 Z_{cx} - k_f^2 Z_{fx} = (\partial/\partial x)\nabla\cdot(\vec{Z}_f - \vec{Z}_c) \qquad (2.5a)$$

$$k_c^2 Z_{cz} - k_f^2 Z_{fz} = (\partial/\partial z)\nabla\cdot(\vec{Z}_f - \vec{Z}_c) \qquad (2.5b)$$

$$(\partial/\partial y)[Z_{cz} - N_{fc} Z_{fz}] = (\partial/\partial z)[Z_{cy} - N_{fc} Z_{fy}] \qquad (2.5c)$$

$$(\partial/\partial x)[Z_{cy} - N_{fc} Z_{fy}] = (\partial/\partial y)[Z_{cx} - N_{fc} Z_{fx}] \qquad (2.5d)$$

These conditions on potential are impractical, because many components appear in each. Following the meritable plan of Sommerfeld [15], consider the independent effects of each current-source component, noting that not all potential components are required to represent the EM field due to each component of current. Then construct, by superposition, boundary conditions for a general current source having all three components.

Case (a): $\vec{J} = \hat{y}J_y$

Conjecture that the total fields are determined by $\vec{Z}=\hat{y}Z_y$ in each region. In this instance the general boundary conditions (2.5) reduce significantly. Equality of tangential derivatives (i.e., those with respect to x and z), for all x and z at y=0, leads to the following conclusions:

$$Z_{cy} = N_{fc}Z_{fy} \tag{2.6a}$$

$$(\partial/\partial y)[Z_{cy}-Z_{fy}] = 0 \tag{2.6b}$$

Case (b): $\vec{J} = \hat{x}J_x$

A naive conjecture that $\vec{Z}=\hat{x}Z_x$ is adequate in this case leads to a mathematical contradiction; therefore, the boundary conditions cannot be satisfied. Include the normal component of $\vec{Z}$ as well, ie., let $\vec{Z}=\hat{x}Z_x+\hat{y}Z_y$, giving

$$(\partial/\partial y)[Z_{cx}-N_{fc}Z_{fx}] = 0 \tag{2.7a}$$

$$(\partial/\partial y)[Z_{cy}-Z_{fy}] = (\partial/\partial x)[Z_{fx}-Z_{cx}] \tag{2.7b}$$

Case (c): $\vec{J} = \hat{z}J_z$

This case is similar to (b); let $\vec{Z}=\hat{z}Z_z+\hat{y}Z_y$ and arrive at

$$(\partial/\partial y)[Z_{cz}-N_{fc}Z_{fz}] = 0 \tag{2.8a}$$

$$(\partial/\partial y)[Z_{cy}-Z_{fy}] = (\partial/\partial z)[Z_{fz}-Z_{cz}] \tag{2.8b}$$

Case (d): $\vec{J} = \hat{x}J_x + \hat{y}J_y + \hat{z}J_z$

General boundary conditions at y=0 are obtained by combining the outcomes of cases (a), (b), and (c). The final results, which show coupling between normal and tangential potential components, are:

$$Z_{cx} = N_{fc}Z_{fx} \tag{2.9a}$$

$$Z_{cy} = N_{fc}Z_{fy} \tag{2.9b}$$

$$Z_{cz} = N_{fc}Z_{fz} \tag{2.9c}$$

$$(\partial/\partial y)[Z_{cx} - N_{fc}Z_{fx}] = 0 \tag{2.9d}$$

$$(\partial/\partial y)[Z_{cz} - N_{fc}Z_{fz}] = 0 \tag{2.9e}$$

$$(\partial/\partial y)[Z_{cy} - Z_{fy}] = (1-N_{fc})[(\partial/\partial x)Z_{fx} + (\partial/\partial z)Z_{fz}) \tag{2.9f}$$

2.5.2 Conditions at Film/Conductor Interface

Next, consider the interface at y=-t. Vanishing tangential components of electric intensity imply

$$k_f^2 Z_{fx} + (\partial/\partial x)\nabla\cdot\vec{Z}_f = 0 \tag{2.10a}$$

$$k_f^2 Z_{fz} + (\partial/\partial z)\nabla\cdot\vec{Z}_f = 0 \tag{2.10b}$$

Again, each component of current density receives separate treatment.

Case (a): $\vec{J} = \hat{y}J_y$

Let $\vec{Z}=\hat{y}Z_y$ represent the EM fields. Setting $E_{fx}=0$ and $E_{fz}=0$ at the conducting interface yields

$$(\partial^2/\partial x\partial y)Z_{fy} = 0 \qquad (2.11a)$$

$$(\partial^2/\partial z\partial y)Z_{fy} = 0 \qquad (2.11b)$$

From vanishing of both tangential derivatives in (2.11) everywhere on the interface,

$$(\partial/\partial y)Z_{fy} = 0 \qquad (2.12)$$

Case (b): $\vec{J} = \hat{x}J_x$

Let $\vec{Z}=\hat{x}Z_x+\hat{y}Z_y$. Implement the same conditions as in case (a) to get

$$Z_{fx} = 0 \qquad (2.13a)$$

$$(\partial/\partial y)Z_{fy} = 0 \qquad (2.13b)$$

Case (c): $\vec{J} = \hat{z}J_z$

Let $\vec{Z}=\hat{z}Z_z+\hat{y}Z_y$. Use the results of (b), with radial slab symmetry (i.e., rotation of coordinates), to arrive at

$$Z_{fz} = 0 \qquad (2.14a)$$

$$(\partial/\partial y)Z_{fy} = 0 \qquad (2.14b)$$

Case (d): $\vec{J} = \hat{x}J_x + \hat{y}J_y + \hat{z}J_z$

General boundary conditions for y=-t are secured by linearity; specific contributions to $\partial Z_{fy}/\partial y$ are summed, as are contributions (all zero) to Z_{fx} and Z_{fz}. The results,

$$Z_{fx} = 0 \qquad (2.15a)$$

$$Z_{fz} = 0 \qquad (2.15b)$$

$$(\partial/\partial y)Z_{fy} = 0 \qquad (2.15c)$$

show a lack of coupling between normal and tangential potential components.

2.6 Integral Representation for Hertz Potential

Integral representations for components of potential are created via the two-dimensional Fourier transform or, alternately, by continuous superposition of plane waves with suitable spectral amplitudes. Care is taken not to transform on y, however, since substitutions into boundary conditions at y=0 and y=-t are imperative.

Let $F\{\ \}$ and $F^{-1}\{\ \}$ denote two-dimensional Fourier and inverse Fourier transform operations. The spatial/spatial-frequency domain variable pairs are (x,u_x) and (z,u_z), with the transforms defined as

$$F\{q\} = Q = \iint q(x,y,z)\exp[-j(u_x x+u_z z)]dxdz \qquad (2.16a)$$

$$F^{-1}\{Q\} = q = (1/2\pi)^2 \iint Q(u_x,y,u_z)\exp[j(u_x x+u_z z)]du_x du_z \tag{2.16b}$$

It should be stressed that the ensuing development is valid only for sources in the cover medium. In a later chapter on the continuous spectrum, expressions for waves excited by sources in the film layer are needed; however, that development need not be as general as the present one, and is of more limited and specific interest. Study of sources in the film layer is therefore deferred to Chapter 5.

Primary potential waves satisfy the inhomogeneous Helmholtz equation

$$\nabla^2 \vec{Z}_{cp} + k_c^2 \vec{Z}_{cp} = -\vec{J}/A_c \tag{2.17}$$

where $A_c = j\omega\varepsilon_c$. Primary waves are those excited in a hypothetical unbounded region having permittivity of the cover (see Figure 4). The solution of (2.17) proceeds by standard Green's function techniques, giving the principal Green's function:

$$G_p(r,r') = \iint \frac{\exp[j\vec{L}\cdot(\vec{r}-\vec{r}')]\exp[-p_c|y-y'|]d^2L}{2A_o p_c} \tag{2.18}$$

where $A_o=(2\pi)^2$. Here $p_c^2(L)=L^2-k_c^2$ is a wavenumber parameter, $\vec{L}=\hat{x}u_x+\hat{z}u_z$ is a vector 2-d spatial frequency, and $d^2L=du_x du_z$. It is noted that (2.18) is just an integral representation for elementary, outward-traveling, spherical waves. By weighted superposition, the primary

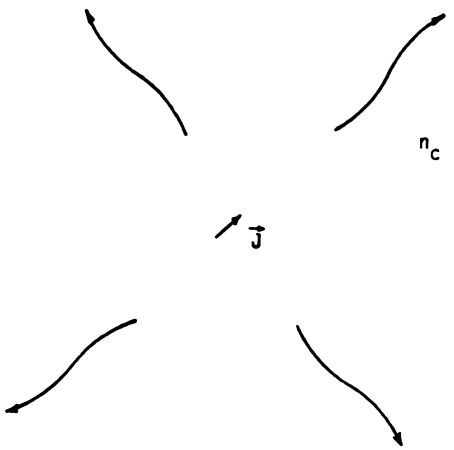

Figure 4. Principal wave of Hertz potential.

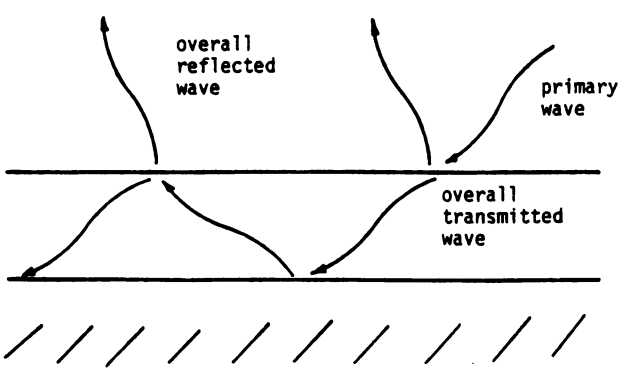

Figure 5. Transmitted and reflected potential waves.

potential wave is

$$\vec{Z}_{cp}(\vec{r}) = (1/A_c)\int_V \vec{J}(\vec{r}')G_p(\vec{r},\vec{r}')dv' \qquad (2.19)$$

Scattered (reflected or transmitted) potential waves are, by definition, source-free. A generic form can be derived to represent the scattered Hertz potentials. Their components (designated by subscript i=x,y,z) satisfy

$$\nabla^2 Z_{i\alpha}^s + k^2 Z_{i\alpha}^s = 0 \qquad (2.20)$$

where α=c,f for cover and film regions. Substitute, using (2.16), for $Z_{i\alpha}^s$ in terms of $F^{-1}\{F\{Z_{i\alpha}^s\}\}$. Pass the x and z derivatives of the Laplacian through integrals and carry them out on the integrand; these operations are easy due to the integrand's exponential form. Then the Fourier transform theorem gives an ordinary differential (in the y-variable) equation for $F\{Z_{i\alpha}^s\}$, which has solutions

$$F\{Z_{i\alpha}^s(\vec{L},y)\} = W_{i\alpha}^s(\vec{L})\exp(\pm p_\alpha y) \qquad (2.21)$$

where $p_\alpha^2=p_\alpha^2(\vec{L})=L^2-k_\alpha^2$ is the transverse wavenumber parameter. The prototype solution for scattered waves of Hertz potential is:

$$Z_{i\alpha}^s(\vec{r}) = (1/A_0)\iint W_{i\alpha}^s(\vec{L})\exp(j\vec{L}\cdot\vec{r})\exp[\pm p_\alpha y]d^2L \qquad (2.22)$$

Finally, requiring that traveling waves suffer decay, total

solutions for Hertz potential are formed. In the cover,

$$Z_{ci} = \int_V \frac{J_i}{A_c} \iint \frac{\exp[j\vec{L}\cdot(\vec{r}-\vec{r}')]\exp[-p_c|y-y'|]d^2L dV}{2A_o p_c} + (1/A_o)\iint W_{cri}(\vec{L})\exp(j\vec{L}\cdot\vec{r})\exp[-p_c y]d^2L \tag{2.23}$$

where $W_{cri}(\vec{L})$ is the overall reflected-wave amplitude spectrum in the cover. In the film,

$$Z_{fi} = (1/A_o)\iint \exp(j\vec{L}\cdot\vec{r})\{W_{fti}(\vec{L})\exp[p_f y]+W_{fri}(\vec{L})\exp[-p_f y]\}d^2L \tag{2.24}$$

where $W_{fti}(\vec{L})$ and $W_{fri}(\vec{L})$ are unknown amplitude spectra for waves transmitted and reflected in the film. Waves affiliated with these spectral coefficients are suggested by Figure 5.

2.7 Hertz Potential Green's Dyad

Nine boundary conditions derived in section 2.5 provide for evaluation of the overall spectral amplitudes "W". Their application and subsequent algebraic reduction lead to concise statement [11] of results in Green's dyadic form.

It is convenient to express Hertz potentials in terms of a Green's dyadic $\bar{\bar{G}}(\vec{r},\vec{r}')$ composed of principal and reflected parts:

$$\vec{Z}_c = (1/A_c)\int_V \bar{\bar{G}}(\vec{r},\vec{r}')\cdot\vec{J}(\vec{r}')dV' \qquad (2.25)$$

$$\bar{\bar{G}}(\vec{r},\vec{r}') = \bar{\bar{G}}_p(\vec{r},\vec{r}') + \bar{\bar{G}}_r(\vec{r},\vec{r}') \qquad (2.26)$$

Principal Green's dyad $\bar{\bar{G}}_p$ is simply the scalar principal Green's function multiplied by the unit dyad $\bar{\bar{I}}=\hat{x}\hat{x}+\hat{y}\hat{y}+\hat{z}\hat{z}$. Vector directions of primary potentials are therefore determined solely by orientations of source currents. The more intricate reflected Green's dyad $\bar{\bar{G}}_r$ embodies cross-coupling effects produced by the cover/film interface:

$$\bar{\bar{G}}_r(\vec{r},\vec{r}') = \hat{x}G_{rt}\hat{x}+\hat{z}G_{rt}\hat{z}+\hat{y}[(\partial/\partial x)G_{rc}\hat{x}+G_{rn}\hat{y}+(\partial/\partial z)G_{rc}\hat{z}] \qquad (2.27)$$

Subscripts t, n, and c stand for tangential, normal, and coupling, respectively; these signify how vector components of current produce other components of Hertzian potential. The reflected Green's dyad components are

$$\begin{pmatrix} G_{rt} \\ G_{rn} \\ G_{rc} \end{pmatrix} = \iint \begin{pmatrix} R_t \\ R_n \\ C \end{pmatrix} \frac{\exp[j\vec{L}\cdot(\vec{r}-\vec{r}')]\exp[-p_c(y+y')]d^2L}{2A_o p_c} \qquad (2.28)$$

with reflection and coupling coefficients [11] as follows.

$$R_t = A_t/Z_h \qquad (2.29a)$$

$$R_n = A_n/Z_e \qquad (2.29b)$$

$$C = 2p_c(N_{fc}-1)/Z_eZ_h \tag{2.29c}$$

where

$$A_t = p_c - p_f\coth(p_f t) \tag{2.30a}$$

$$A_n = N_{fc}p_c - p_f\tanh(p_f t) \tag{2.30b}$$

$$Z_h = p_c + p_f\coth(p_f t) \tag{2.30c}$$

$$Z_e = N_{fc}p_c + p_f\tanh(p_f t) \tag{2.30d}$$

and

$$p_c^2 = u_x^2 + u_z^2 - k_c^2 \tag{2.31a}$$

$$p_f^2 = u_x^2 + u_z^2 - k_f^2 \tag{2.31b}$$

Note that $Z_h(L)=0$ and $Z_e(L)=0$ are, respectively, eigenvalue equations for TE and TM surface-wave modes of the layered surround; solutions $L=L_b$ of these characteristic equations are named background poles.

2.8 Reflected Green's Dyad for Equal Permittivities

It is instructive to inspect the reflected Green's dyad in the situation where $n_f=n_c$. The refractive index ratio N_{fc} equals unity,

resulting in C=0 and G_{rc}=0. The reflected Green's dyad reduces to $\bar{\bar{G}}_r = \hat{x}G_{rt}\hat{x} + \hat{y}G_{rn}\hat{y} + \hat{z}G_{rt}\hat{z}$ with $p_f = p_c$. With some algebraic simplification, it is shown to be proportional to the dyad $-\hat{x}\hat{x}+\hat{y}\hat{y}-\hat{z}\hat{z}$. Moreover, a phase factor $\exp[-2p_c t]$ appears explicitly, giving the expected propagation delay as a function of the distance from source to conducting plane.

In this special case, therefore, the reflected Green's dyad predicts classical equivalent image currents. The image is placed at a distance t below the conducting plane, with its normal (y) component in the same direction as the primary source, and tangential (x and z) components reversed.

2.9 Green's Dyad Source-point Singularity

A thorough investigation of the Green's function source-point singularity is worthwhile, as it brings out an interesting physical interpretation involving charges and currents. For completeness, salient points of the development for a surface-current source distribution are given in this section.

Let currents, described by density $\vec{K}(\vec{r})$, be located on a surface S. S has outer boundary contour C_o. Assume that $\vec{K}$ is a continuous function everywhere on S except at the boundary C_p of patch S_p. Let $\hat{n}$ be the outward-directed unit normal vector from S, in the plane of S. First, consider the electric field associated with the principal Green's function only.

Despite the double-integral formulation of equation (2.18), it is also known that G_p can be represented simply by $G_p = \exp(-jk_c R)/4\pi R$, where $R = |\vec{r} - \vec{r}'|$ is the distance from source point to observation point;

this reveals the source-point singularity strength experienced when $\vec{r}=\vec{r}'$. Due to the singularity, integrals involving G_p must be done as improper integrals, taking care not to allow $|\vec{r}-\vec{r}'|=0$ to occur. To this end it is necessary to further exclude from S a limitingly small circle, of radius d, centered on the location $\vec{r}$; call the excluded region S_d with boundary C_d, noting that $\hat{n}$ is directed into S_d.

From equations (2.2a), (2.25) and (2.26), the principal electric field component is

$$\vec{E}_p = (1/A_c)\{k_c^2 \int_S G_p(\vec{r},\vec{r}')\vec{K}(\vec{r}')dS' + \nabla\nabla\cdot\int_S G_p(\vec{r},\vec{r}')\vec{K}(\vec{r}')dS'\} \tag{2.32}$$

where, in the limit as d approaches zero, S is composed of the two portions $S=\{S-S_d-S_p\}+S_p$. It is immediately clear that, in (2.32), the first term is related to vector potential produced by current. The second term relates to scalar potential produced by electric charge; this is evident after passing the divergence operator through the spatial integral, with subsequent identification of the second term as the gradient of a scalar potential. Manipulation of the scalar potential integrand yields

$$\begin{aligned}\nabla\cdot[G_p(\vec{r},\vec{r}')\vec{K}(\vec{r}')] &= G_p(\vec{r},\vec{r}')\,\nabla\cdot\vec{K}(\vec{r}') + \nabla G_p(\vec{r},\vec{r}')\cdot\vec{K}(\vec{r}') \\ &= -\nabla' G_p(\vec{r},\vec{r}')\cdot\vec{K}(\vec{r}') \\ &= -\nabla'\cdot[G_p(\vec{r},\vec{r}')\vec{K}(\vec{r}')] + G_p(\vec{r},\vec{r}')\,\nabla'\cdot\vec{K}(\vec{r}')\end{aligned} \tag{2.33}$$

The divergence theorem in primed coordinates now applies to the first term to give contour integrals of functions $\hat{n}' \cdot \vec{K}$ (clearly equivalent line charges) around the three contours C_o, C_p, and C_d. The second term, by the surface continuity equation, yields superpositions over surface charges on S. It is found, moreover, that as d approaches zero the contribution from the (artificially introduced) line charge at C_d vanishes.

Treatment of the reflected component of electric field is initially not as easy. This is due to the more complicated dyadic form of the reflected Green's function. From equation (2.27) with $\vec{K} = \hat{x}K_x + \hat{z}K_z$, the reflected scalar potential integrand becomes

$$\nabla \cdot [\bar{G}_r \cdot \vec{K}] = [K_x(\partial/\partial x)G_{rt} + K_z(\partial/\partial z)G_{rt}] + [K_x(\partial/\partial x)(\partial/\partial y)G_{rc} + K_z(\partial/\partial z)(\partial/\partial y)G_{rc}] \tag{2.34}$$

The right-hand side can be written $\nabla_t \tilde{G}_r \cdot \vec{K}$, where $\tilde{G}_r = G_{rt} + (\partial/\partial y)G_{rc}$ and ∇_t is the transverse gradient operation involving only partial derivatives on x and z. Referring to equation (2.33), this is of exactly the form required to carry through steps analogous to those for G_p.

Besides offering a convenient physical picture of equivalent sources that produce electric fields, the source-point singularity development outlined here represents an alternative formulation for later problems in terms of unknown charges and currents (instead of just unknown currents). Removing derivatives from the Green's function and placing them onto currents is a highly recommended method of

avoiding increasing the Green's function singularity; more is said of this, in connection with integration by parts, in Chapter 4.

2.10 Conclusion

Electromagnetic fields, maintained by currents over layered conductor/film media, are given by integro-differential operations on the Hertz potential Green's dyad developed in this chapter. The Green's dyad formulation accounts rigorously for layered media effects. The EM fields are, in addition, subject to further boundary conditions imposed by any conducting devices resting over the film. In the following chapter, such boundary conditions are carried out for the infinite microstrip line, resulting in an integral equation for unknown surface currents on the strip.

CHAPTER III

PROPER MODE SPECTRUM FOR MICROSTRIP LINE

3.1 Introduction

Propagation modes of axially-uniform microstrip lines are quantified based upon a general electric field integral equation (IE). IE construction proceeds through the Hertz potential Green's dyad, equation (2.26), developed in Chapter 2. A subsequent complex plane analysis reveals naturally the proper spectrum for microstrip modes, including the discrete and continuous spectra.

3.2 General Integral Equation for Electric Field

Suppose microstrip excitation is provided through an impressed electric field $\vec{E}^i$ maintained by primary current source $\vec{J}^e$. The impressed field induces a system of surface currents, described by density $\vec{K}$, on conducting strip lines. Induced currents maintain a scattered field $\vec{E}^s$. See Figure 6. At any point $\vec{r}$, the total field is given by superposition: $\vec{E}=\vec{E}^i+\vec{E}^s$. The boundary condition at a conductor, $\hat{t}\cdot\vec{E}=0$, implies $\hat{t}\cdot\vec{E}^s(\vec{r})=-\hat{t}\cdot\vec{E}^i(\vec{r})$ at the microstrip surface; this is the basis for constructing an electric field integral equation (EFIE) for unknown surface currents $\vec{K}(\vec{r})$. Assuming time-harmonic excitation,

$$\hat{t}\cdot\{k_c^2 + \nabla\nabla\cdot\}\int_S \bar{G}(\vec{r},\vec{r}')\cdot\vec{K}(\vec{r}')dS' = -A_c\hat{t}\cdot\vec{E}^i(\vec{r}) \qquad (3.1)$$

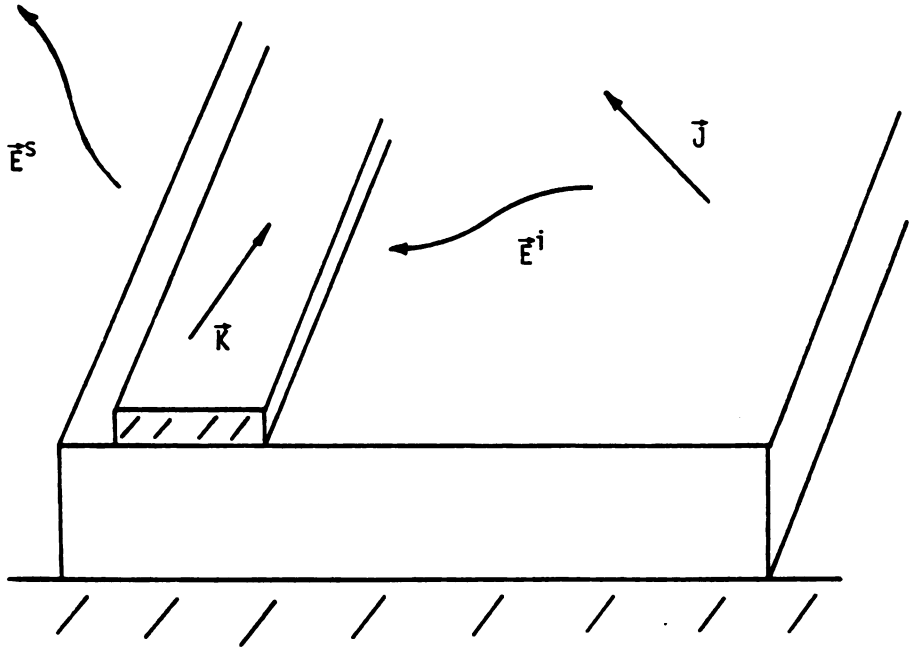

Figure 6. Impressed and scattered fields.

Particularily well-suited to moment method solutions, this EFIE is the mathematical foundation for all topics addressed in this thesis. It is Fourier-transformed in the next section.

3.3 General EFIE in the Fourier Transform Domain

For axially-invariant microstrip systems,

$$\hat{t}\cdot\{k_c^2 + \nabla\nabla\cdot\} \int_C dl' \int dz' \bar{\bar{G}}(\vec{\rho},\vec{\rho}';z-z')\cdot\vec{K}(\vec{\rho}',z') = -A_c\hat{t}\cdot\vec{E}^i(\vec{\rho},z) \tag{3.2}$$

where $\vec{\rho}$ is the 2-d transverse (x-y plane) position vector, and C denotes periphery contours of microstrip conductors. Take a Fourier transform on z, noting the axial (z) integral is purely convolutional, to arrive at a two dimensional EFIE:

$$\hat{t}\cdot\{k_c^2 + \tilde{\nabla}\tilde{\nabla}\cdot\} \int_C \bar{\bar{g}}(\vec{\rho},\vec{\rho}')\cdot\vec{k}(\vec{\rho}';u_z)dl' = -A_c\hat{t}\cdot\vec{e}^i(\vec{\rho},u_z) \tag{3.3}$$

where u_z is the transform variable for z. Transformed quantities in (3.3) are stated in lower case letters; furthermore, it is understood that the differentiation theorem has mapped partial derivatives with respect to z into multiplications by ju_z (new symbol $\tilde{\nabla}$).

Scalar components of the principal and reflected Green's dyadics transform to

$$g_p = \int \frac{\exp[ju_x(x-x')]\exp[-p_c|y-y'|]du_x}{4\pi p_c} \tag{3.4}$$

$$\begin{pmatrix} g_{rt} \\ g_{rn} \\ g_{rc} \end{pmatrix} = \int \begin{pmatrix} R_t \\ R_n \\ C \end{pmatrix} \frac{\exp[ju_x(x-x')]\exp[-p_c(y+y')]du_x}{4\pi p_c} \qquad (3.5)$$

These expressions are useful for applications in Chapters 4, 5, and 6.

3.4 Identification of Propagation-mode Spectrum

The propagation-mode spectrum is identified from inverse transforms of solutions to the 2-d EFIE for $\vec{k}$, equation (3.3). Inverse Fourier transforming,

$$\vec{K}(\vec{r}) = F^{-1}\{\vec{k}\} = (1/2\pi)\int \vec{k}(\vec{\rho},u_z)\exp(ju_z z)du_z \qquad (3.6)$$

Consider wavenumber parameters p_c and p_f, found by taking square roots of p_c^2 and p_f^2; they are given generically by

$$p = (u_x^2+u_z^2-k^2)^{1/2} = (u_x^2+\gamma^2)^{1/2} \qquad (3.7)$$

where

$$\gamma = (u_z^2-k^2)^{1/2} = [(u_z-k)(u_z+k)]^{1/2} \qquad (3.8)$$

Care is taken to choose correct branch cuts for these potentially multivalued functions of u_z so decaying wave solutions are generated, i.e., so $\mathrm{Re}\{p_c\}>0$ and $\mathrm{Re}\{p_f\}>0$. As p_c and p_f exist within an integration spanning all u_x, $u_x=0$ will occur; this imposes $\mathrm{Re}\{\gamma_c\}>0$ and $\mathrm{Re}\{\gamma_f\}>0$. The square roots γ_c and γ_f have branch point singularities at $u_z=\pm k_c$ and $u_z=\pm k_f$. However, all functions of p_f in the integral

representation for the Green's dyad are even functions; see equation (2.30). Consequently branch points at $\pm k_f$ are not implicated; only those at $\pm k_c$ are relevant. Considering γ_c in detail,

$$\gamma_c^2 = (u_{zr}^2 - u_{zi}^2 - k_{cr}^2 + k_{ci}^2) + j2(u_{zr}u_{zi} - k_{cr}k_{ci}) \tag{3.9}$$

where subscripts r and i denote real and imaginary parts. It is understood that $k_{ci} = \mathrm{Im}\{k_c\} < 0$ for lossy dielectric media.

Now $\mathrm{Re}\{\gamma_c\} > 0$ implies $|\arg\{\gamma_c\}| < 90^o$, or $|\arg\{\gamma_c^2\}| < 180^o$, and therefore the boundary line for the proper Riemann sheet is the negative real axis defined by $\mathrm{Im}\{\gamma_c^2\} = 0$ and $\mathrm{Re}\{\gamma_c^2\} < 0$. $\mathrm{Im}\{\gamma_c^2\} = 0$ and (3.9) lead to a hyperbolic branch cut,

$$u_{zi} = k_{cr}k_{ci}/u_{zr} \tag{3.10}$$

emanating from the branch points. The remaining condition, $\mathrm{Re}\{\gamma_c^2\} < 0$, specifies that portion of the hyperbola asymptotic to the imaginary axis (where $u_{zi}^2 > k_{ci}^2$ and $u_{zr}^2 < k_{cr}^2$). See Figure 7 for a graphical representation of the suitably cut u_z-plane, specialized to the low-loss limit.

The singularities of the transform-domain surface current are: (1) branch points at $\pm k_c$ through dependence on the Green's dyad, and (2) surface-wave poles at $\pm u_{zm}$; m=1,2,...,p,..., M. With appropriate hyperbolic branch cuts along C_b, the real-axis Fourier inversion integral is deformed into the complex u_z plane and subjected to Cauchy's Integral Theorem [16]. Let semicircles of infinite radius in the upper and lower half-plane provide alternatives for closure of the

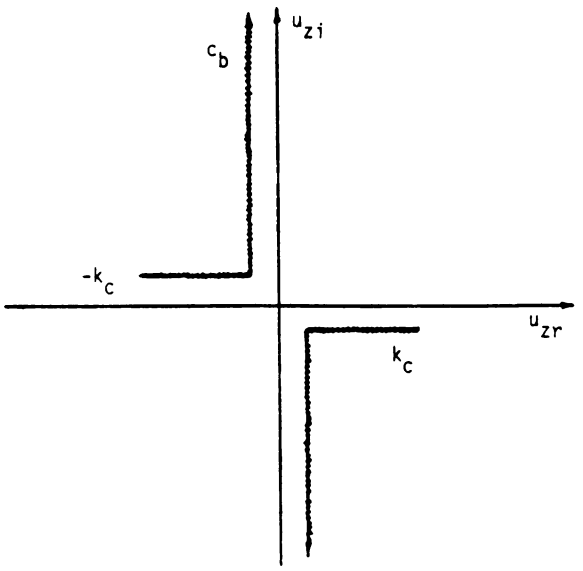

Figure 7. Branch cuts in complex u_z plane.

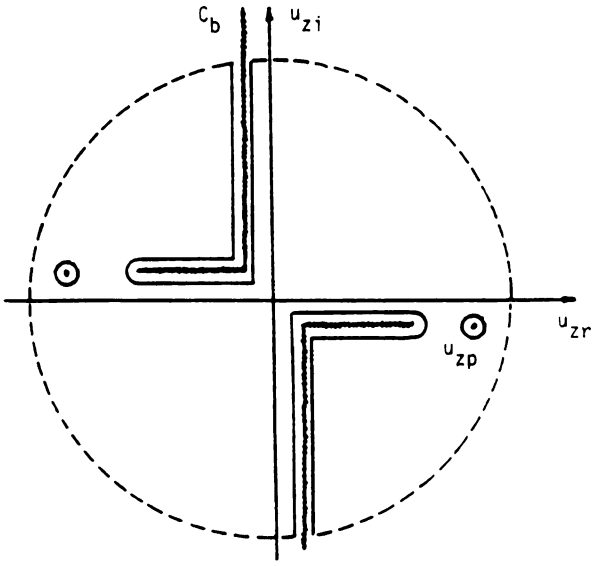

Figure 8. Integration contour closure.

integration contour. See Figure 8. No contribution from the chosen infinite semicircle should be made. From

$$\int_C \vec{k}\, \exp(ju_z z)du_z = \int_C \vec{k}\, \exp(-u_{zi} z)\exp(ju_{zr} z)du_z \qquad (3.11)$$

the correct selection of closing contour is to choose: (1) upper half plane closure if $z>z'$, and (2) lower half plane closure if $z<z'$.

By Cauchy's residue theorem,

$$\vec{K} = \sum_m a_m \vec{k}_m \exp(ju_{zm} z) - (1/2\pi)\int_{C_b} \vec{k}\, \exp(ju_z z)dz \qquad (3.12)$$

where

$$a_m \vec{k}_m \exp(ju_{zm} z) = -j\mathrm{Res}_m\{\vec{k}\, \exp(ju_z z)\} \qquad (3.13)$$

Suggested in (3.12) are a discrete sum of guided propagation modes, and a superposition of continuous spectral components leading to the radiation field. Therefore, a rigorous complex plane analysis reveals the proper microstrip mode spectrum.

3.5 Forced and Unforced EFIE Solutions

It is conjectured that propagation modes of the strip are affiliated with simple pole singularities. That is, $\vec{k}$ can be expressed as an analytic function divided by terms of the form (u_z-u_{zm}). However, the impressed electric field does not necessarily share these transform-domain singularities. Therefore, when $u_z=u_{zm}$, the analytic

factor in $\vec{k}$ must satisfy a homogeneous IE to maintain an indeterminate form on the LHS of (3.3). Understanding $\vec{k}$ now to mean only the analytic part of the current density function,

$$\hat{\tilde{t}}\cdot\{k_c^2 + \tilde{\tilde{\nabla}}\tilde{\tilde{\nabla}}\cdot\} \int_C \bar{\bar{g}}\cdot\vec{k}(\vec{\rho},u_{zm})dl' = 0 \qquad (3.14)$$

for propagation modes. Moreover, as propagation modes are homogeneous solutions of the EFIE, forced solutions must be continuous radiation modes.

3.6 Conclusion

Discrete and continuous modes comprise the proper spectrum of microstrip surface currents. This observation arises naturally as the outcome of complex-plane contour integration. Discrete modes are terms in a residue series; the continuous spectrum results from imperative detours around branch cuts.

The importance of this conceptual classification of microstrip modes resides in its possibility for future application to practical problems. In case a discontinuity is involved, for example, one might expect radiation fields near the discontinuity to be produced by, and therefore relate strongly to, the continuous spectrum -- away from the discontinuity the discrete modes would probably dominate.

It is also demonstrated in this chapter that discrete modes are solutions of the homogeneous transform-domain EFIE (3.14), while continuous spectral components are forced solutions evaluated at points along the branch cut.

CHAPTER IV

DISCRETE MICROSTRIP MODES

4.1 Introduction

In this chapter, solutions of the homogeneous transform-domain EFIE are sought. These solutions represent discrete microstrip propagation modes. The integral equation is solved for the practical geometry of a very thin strip integrated on the film/cover interface. It should be understood throughout this chapter that the symbol u_z is an abbreviated version of the pole singularity u_{zm}.

4.2 Limiting Case of Thin Microstrip

Assume a very thin strip of width 2W, centered on the coordinate origin and parallel to the z axis. See Figure 9. In this situation, all currents reside at y=0. Source points are therefore located at y=0, as are locations r where the EFIE is enforced:

$$\hat{t}\cdot\{k_c^2 + \tilde{\tilde{\nabla}}\tilde{\tilde{\nabla}}\cdot\} \int_{-w}^{w} \bar{\bar{g}}(x,y;x',0)\cdot\vec{k}(x',u_z)dx' = 0 \qquad (4.1)$$

This holds at y=0 for all x in (-w,w), where $\hat{t}=\hat{x},\hat{z}$ are both tangential to the strip. Evaluation at y=0, subsequent to differentiation, is understood. The surface current density function has in general two components: $\vec{k}=\hat{x}k_x+\hat{z}k_z$.

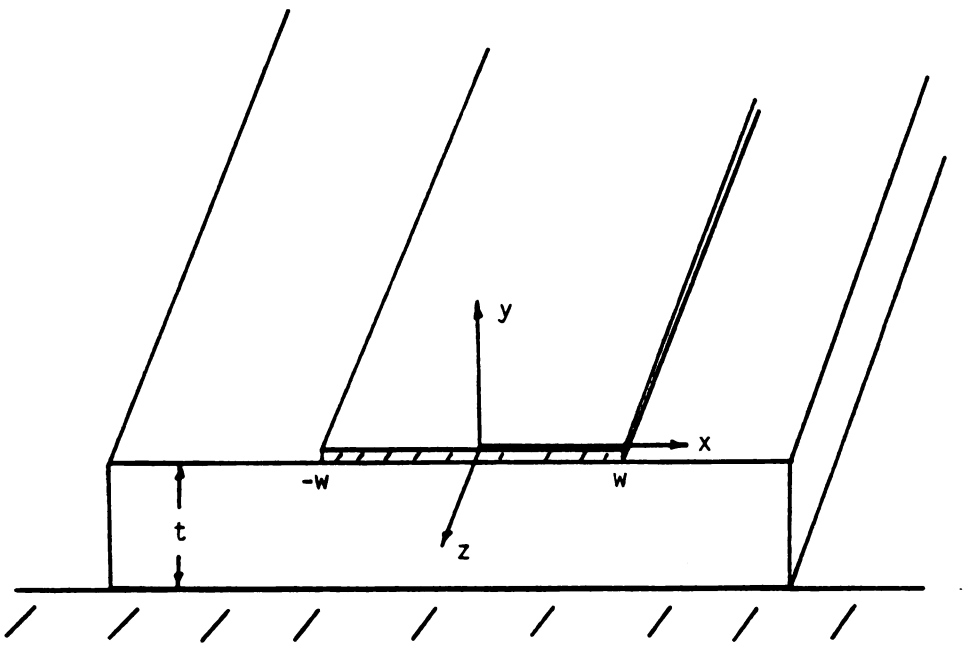

Figure 9. Thin microstrip line.

4.3 Coupled IE's for Current Components

To write explicitly a set of coupled IE's for x and z directed currents, first expand the integrand using

$$\bar{\bar{g}}_r \cdot \vec{k} = \hat{x} g_{rt} k_x + \hat{y}[k_x(\partial g_{rc}/\partial x) + k_z j u_z g_{rc}] + \hat{z} g_{rt} k_z \qquad (4.2)$$

leading to

$$\bar{\bar{g}} \cdot \vec{k} = \vec{k}(g_p + g_{rt}) + \hat{y}[k_x(\partial g_{rc}/\partial x) + k_z j u_z g_{rc}] \qquad (4.3)$$

Note also,

$$\hat{x} \cdot (\bar{\bar{g}} \cdot \vec{k}) = (g_p + g_{rt}) k_x \qquad (4.4a)$$

$$\hat{z} \cdot (\bar{\bar{g}} \cdot \vec{k}) = (g_p + g_{rt}) k_z \qquad (4.4b)$$

Coupled IE's for components of surface current, each holding for x in (-w,w), are then:

$$k_c^2 \int_{-w}^{w} (g_p + g_{rt}) k_x dx' + (\partial/\partial x)\, \tilde{\nabla} \cdot \int_{-w}^{w} \bar{\bar{g}} \cdot \vec{k} dx' = 0 \qquad (4.5a)$$

$$k_c^2 \int_{-w}^{w} (g_p + g_{rt}) k_z dx' + j u_z\, \tilde{\nabla} \cdot \int_{-w}^{w} \bar{\bar{g}} \cdot \vec{k} dx' = 0 \qquad (4.5b)$$

where, again, evaluation at y=y'=0 is understood.

In working with equations (4.5a) and (4.5b), the immediate

interchange of derivative and integral operations is tempting. However, such exchanges are often associated with problems of integral convergence; this occurs particularly in the second term of (4.5b). Interchanges are therefore done with caution, and are avoided in the case of (4.5b).

4.4 Dominant Axial Current Approximation

Expectedly [3], $|k_x| << |k_z|$. In this approximation both IE's cannot be satisfied, so discard the equation arising from the e_x boundary condition. The remaining IE, equation (4.5b), with

$$\bar{\bar{g}} \cdot \vec{k} = [\hat{y} j u_z g_{rc} + \hat{z}(g_p + g_{rt})] k_z \tag{4.6}$$

is enforced at y=y'=0 for all x in (-w,w). Passing the divergence operator through the integral,

$$\tilde{\nabla} \cdot \bar{\bar{g}} \cdot \vec{k} = j u_z [\partial g_{rc}/\partial y + (g_p + g_{rt})] k_z \tag{4.7}$$

The EFIE is

$$\int_{-w}^{w} [-\gamma_c^2 (g_p + g_{rt}) - u_z^2 (\partial g_{rc}/\partial y)] k_z dx' = 0 \tag{4.8}$$

where $\gamma_c^2 = u_z^2 - k_c^2$. Further simplification proceeds via symmetry. Write the LHS integral as a sum of two integrations: one spanning (-w,0), the other (0,w). Then make a change of variable u=-x' in the first integral. By physical symmetry $k_z(x)$ must be either even or odd about

the microstrip centerline, prompting decomposition of $k_z(x)$ into even and odd modes:

$$k_z(-x) = Sk_z(x) = \begin{cases} k_z(x) \text{ for even modes} \\ -k_z(x) \text{ for odd modes} \end{cases} \tag{4.9}$$

where S=1 for even modes and S=-1 for odd modes. The EFIE is now enforced over the right half of the strip, (0,w):

$$\int_0^w \{[-\gamma_c^2(g_p+g_{rt})-u_z^2\partial g_{rc}/\partial y]S\Big|_{(x' \text{ replaced by } -x')} + [-\gamma_c^2(g_p+g_{rt})-u_z^2\partial g_{rc}/\partial y]\}k_z(x')dx' = 0 \tag{4.10}$$

with y=y'=0 understood subsequent to differentiation. The EFIE is now written compactly:

$$\int_0^w [T(x,x')+ST(x,-x')]k_z(x')dx' = 0 \tag{4.11}$$

where

$$T = \gamma_c^2(g_p+g_{rt})+u_z^2(\partial g_{rc}/\partial y)\Big|_{(y=y'=0)}$$

$$= (1/4\pi)\int \exp[ju_x(x-x')]\{\gamma_c^2[(1+R_t)/p_c]-u_z^2C\}du_x \tag{4.12}$$

Let

$$U = [\gamma_c^2(1+R_t)/p_c]-u_z^2C = 2[\gamma_c^2-u_z^2p_c(N_{fc}-1)/Z_e]/Z_h \qquad (4.13)$$

and drop multiplicative constants to get

$$\int_0^w \int U\{\exp[ju_x(x-x')]+S\exp[ju_x(x+x')\}du_xk_z(x')dx' = 0 \qquad (4.14)$$

4.4.1 Solution by Pulse Galerkin's Method

In preparation for moment method [17] solution, rewrite the EFIE slightly:

$$\int_0^w \int U\exp(ju_xx)\{\exp(-ju_xx')+S\exp(ju_xx')\}du_xk_z(x')dx' = 0 \qquad (4.15)$$

Subdivide (0,w) into N partitions, each of width 2h, and let the center point of the n'th partition be x_n. The n'th partition is (x_n-h, x_n+h). A set of N nonoverlapping pulse functions, defined by

$$P_n(x) = \begin{cases} 1 \ . \ . \ . \text{ if } (x_n-h)<x<(x_n+h) \\ 0 \ . \ . \ . \text{ otherwise} \end{cases} \qquad (4.16)$$

is the basis for expansion of the unknown $k_z(x)$ as

$$k_z(x) = \sum_{n=1}^{N} k_{zn}P_n(x) \qquad (4.17)$$

where k_{zn} is the n'th expansion coefficient. Substituting this into the EFIE,

$$\int_0^w \int U\exp(ju_x x)\{\exp(-ju_x x')+S\exp(ju_x x')\}du_x \sum_{n=1}^{N} k_{zn} P_n(x)dx' = 0 \tag{4.18}$$

$$\sum_{n=1}^{N} k_{zn} \int \exp(ju_x x)[\sin(u_x h)/u_x]\{\exp(-ju_x x_n)+S\exp(ju_x x_n)\}du_x = 0 \tag{4.19}$$

Galerkin's method expansion and testing functions are identical, so invoke the following testing operation:

$$\int_0^w \{\ \}P_m(x)dx \quad \text{for } m=1,\ldots,N \tag{4.20}$$

Integrating the pulse functions into the x-dependent exponential factors, combining exponentials, and dropping overall left-hand side multiplicative constants, a matrix equation,

$$\sum_{n=1}^{N} k_{zn} A_{mn}(u_z) = 0 \quad \text{for } m=1,\ldots,N \tag{4.21}$$

is obtained for the N unknown expansion coefficients. The mn'th matrix element is given by

$$A_{mn}(u_z) = \int UT^2\{\exp[u_x(x_m-x_n)]+S\exp[u_x(x_m+x_n)]\}du_x \tag{4.22}$$

where $T=\sin(u_x h)/u_x$.

4.4.2 Physical Implications of Surface-wave Poles

As stated in Chapter 2 the layered background has an eigenmode spectrum with surface-wave and radiation modes. Its surface-wave poles occur in functions R_t, R_n, and C of the reflected Green's dyad. Components of $\bar{\bar{g}}$ are represented above as real-line spectral integrals. Note, however, that in a complex u_x plane analogous to Chapter 3 the poles would produce residues (surface-wave modes), while slab radiation modes would arise from branch cuts. In this way the Green's dyad formulation includes all relevant information about slab eigenmodes .

In a strictly real-line integral format, under certain conditions, poles of R_t, R_n and C are encountered along the real integration axis. If they are isolated within small neighborhoods, and the integration is done analytically over the small intervals, the results equal the residue contributions of the preceding paragraph. (By inference, then, the remaining integration away from poles represents an expansion in slab radiation modes.)

This represents a possible mechanism for coupling of microstrip modes to surface waves of the slab. In the present work, physical parameters are chosen carefully to assure that only the TM_0 pole can be present. More is said of this in the following section.

4.4.3 Computational Methods

A FORTRAN program, using complex arithmetic, provides numerical solutions for the moment method problem formulated above. Surface-wave eigenvalues $u_z=u_{zm}$ are searched for in the complex plane via

secant method. Computation of Sommerfeld-type integrals is regarded a difficult hurdle in layered-media problems [18]. Numerical integration of matrix elements $A_{mn}(u_z)$ is done in several steps. It is observed through numerical experimentation that the integrands generally undergo a transition in behavior at $u_x=k_f$. Acknowledging the possible presence of the TM_0 surface-wave pole (a $Z_e(L)= 0$ solution) within $(0,k_f)$, a small region centered on the TM_0 pole is excluded from the interval. An analytically determined term is added to compensate; derivation of this term appears in Appendix B. Adaptive Simpson's rule accomplishes numerical integration over this first interval. Over the remaining interval from k_f to infinity, integration is handled step-by-step in periods of the slowest-oscillating contribution. Within these steps, subdivision is done into periods of the most rapidly oscillating contribution; these are integrated by 9-point Gaussian quadrature. Several data items are required as input. Film and cover media refractive indices n_f and n_c are entered. Wavelength-normalized inputs are required for film thickness t and microstrip half-width w. Surface-wave eigenvalue L for the TM_0 symmetric-slab mode is determined for the given film thickness and refractive indices by a separate program (remembering that the corresponding symmetric slab has thickness 2t). Finally, a value u_{zo} is needed for secant method initiation.

4.5 Solution of Coupled Integral Equations

Proceeding now to the solution for both k_x and k_z, the IE's to be enforced at y=0 for -w<x<w are (4.5a) and (4.5b), restated as

$$(I_z + ju_z J) = 0 \tag{4.23a}$$

$$(I_x + \partial J/\partial x) = 0 \tag{4.23b}$$

in which the following are terms proportional to potentials maintained by currents:

$$I_z = k_c^2 \int_{-w}^{w} g_1 k_z(x')dx' \tag{4.24a}$$

$$I_x = k_c^2 \int_{-w}^{w} g_1 k_x(x')dx' \tag{4.24b}$$

$$J = \tilde{\nabla} \cdot \int_{-w}^{w} \bar{\bar{g}} \cdot \vec{k}\, dx' \tag{4.25}$$

Green's functions appearing in these integral operators are defined by

$$g_1 = g_p + g_{rt} \tag{4.26}$$

$$\bar{\bar{g}} \cdot \vec{k} = \hat{x} k_x g_1 + \hat{z} k_z g_1 + \hat{y}(k_x g_2 + k_z g_3) \tag{4.27}$$

$$g_{1,2,3} = \int \exp[ju_x(x-x')] f_{1,2,3}\, du_x \tag{4.28}$$

where

$$f_1 = [\exp(-p_c|y|)+R_t\exp(-p_c y)]/p_c \tag{4.29a}$$

$$f_{2,3} = jC\exp(-p_c y)(u_{x,z})/p_c \tag{4.29b}$$

Note that f_1 and f_3 are even functions of u_x, while f_2 is odd.

4.5.1 Expansion in Entire-domain Basis Functions

The transform-domain surface continuity equation,

$$\tilde{\nabla}\cdot\vec{k} = \partial k_x/\partial x + ju_z k_z = -j\omega\rho_s(x), \tag{4.30}$$

together with physical symmetry of the charge density function about x=0, implies k_x is (odd,even) in x whenever k_z is (even,odd). Thus it is natural to consider "even" and "odd" (based on the symmetry of k_z) current modes.

Entire-domain basis functions are chosen to represent the coupled surface currents. This choice is intended to reduce moment method matrix size by keeping the number of expansion functions small. Functions k_x and k_z are expanded in power series; following [19], expected edge behaviors are accounted for via multiplicative square root factors:

$$k_z = \sum_n K_{zn} e_{zn}(x) \tag{4.31a}$$

$$k_x = \sum_n K_{xn} e_{xn}(x) \tag{4.31b}$$

$$e_{zn}(x) = (x/w)^n[1-(x/w)^2]^{-1/2} \tag{4.32a}$$

$$e_{xn}(x) = (x/w)^n[1-(x/w)^2]^{+1/2} \qquad (4.32b)$$

The basis functions are understood to be nonzero only for even or odd n values, depending upon modal symmetry. (For example, the z-directed even-mode current is expanded in even powers of x.) Substituting directly into I_z and I_x,

$$I_z = k_c^2 \sum_n K_{zn} \int f_1 \exp(ju_x x) \int_{-w}^{w} e_{zn} \exp(-ju_x x')dx'du_x \qquad (4.33a)$$

$$I_x = k_c^2 \sum_n K_{xn} \int f_1 \exp(ju_x x) \int_{-w}^{w} e_{xn} \exp(-ju_x x')dx'du_x \qquad (4.33b)$$

It is found by inspection that passing the divergence operator through the spatial integral in J does not produce convergence problems. The intent is to carry out the divergence analytically on the integrand of J, which has a form amenable to this:

$$J = \int_{-w}^{w} \tilde{\nabla} \cdot [\bar{\bar{g}} \cdot \vec{k}] \, dx'$$

$$= \int_{-w}^{w} \tilde{\nabla} \cdot [k_z(zg_1+yg_3)+k_x(xg_1+yg_2)]dx'$$

$$= \int_{-w}^{w} \{k_z[ju_z g_1 + \partial g_3/\partial y] + k_x[\partial g_1/\partial x + \partial g_2/\partial y]\}dx'$$

Expanding the currents,

$$J = \sum_n K_{zn}[ju_z \int f_1 \exp(ju_x x) \int_{-w}^{w} e_{zn} \exp(-ju_x x')dx'du_x$$

$$+ (\partial/\partial y) \int f_3 \exp(ju_x x) \int_{-w}^{w} e_{zn} \exp(-ju_x x')dx'du_x]$$

$$+ K_{xn}[\int_{-w}^{w} e_{xn} (\partial/\partial x) \int \exp[ju_x(x-x')]f_1 du_x dx'$$

$$+ (\partial/\partial y) \int f_2 \exp(ju_x x) \int_{-w}^{w} e_{xn} \exp(-ju_x x')dx'du_x] \tag{4.34}$$

Consider the third term in (4.34). Invoking integration by parts removes the x derivative from the Green's function and, using integrand symmetry with respect to x and x', places an x' derivative on the basis function. Increasing the strength of the Green's function singularity is thereby avoided. Evaluation is simplified by noting $e_{xn}(\pm w)=0$.

$$\int_{-w}^{w} e_{xn} (\partial/\partial x) \int \exp[ju_x(x-x')]f_1 du_x dx' =$$

$$\int f_1 \exp(ju_x x) \int_{-w}^{w} e'_{xn} \exp(-ju_x x')dx'du_x \tag{4.35}$$

Make the following definitions:

$$h_{(1,2,3)n} = \int_{-w}^{w} (e_{zn}, e_{xn}, e'_{xn}) \exp(-ju_x x) dx' \qquad (4.36)$$

Then

$$I_z = k_c^2 \sum_n K_{zn} \int f_1 \exp(ju_x x) h_{1n} du_x \qquad (4.37a)$$

$$I_x = k_c^2 \sum_n K_{xn} \int f_1 \exp(ju_x x) h_{2n} du_x \qquad (4.37b)$$

$$J = \sum_n K_{zn} [ju_z \int f_1 \exp(ju_x x) h_{1n} du_x + (\partial/\partial y) \int f_3 \exp(ju_x x) h_{1n} du_x]$$

$$+ \sum_n K_{xn} [\int f_1 \exp(ju_x x) h_{3n} du_x + (\partial/\partial y) \int f_2 \exp(ju_x x) h_{2n} du_x] \qquad (4.38)$$

4.5.2 Galerkin's Method Testing

Invoke the testing operations

$$\int_{-w}^{w} t_{(z,x)m} \{ \} dx$$

with testing functions

$$t_{zm}(x) = (x/w)^m [1-(x/w)^2]^{-1/2} \qquad (4.39a)$$

$$t_{xm}(x) = (x/w)^m[1-(x/w)^2]^{+1/2} \tag{4.39b}$$

The testing functions are understood to be nonzero only for appropriate values of m. Define

$$L_{(1,2,3)m} = \int_{-w}^{w} (t_{zm}, t_{xm}, t'_{xm}) \exp(ju_x x)dx \tag{4.40}$$

Then

$$\int_{-w}^{w} t_{zm}\{I_z\}dx = k_c^2 \sum_n K_{zn} \int f_1 h_{1n} L_{1m} du_x \tag{4.41a}$$

$$\int_{-w}^{w} t_{xm}\{I_x\}dx = k_c^2 \sum_n K_{xn} \int f_1 h_{2n} L_{2m} du_x \tag{4.41b}$$

$$\int_{-w}^{w} t_{zm}\{J\}dx = \sum_n K_{zn}[ju_z \int f_1 h_{1n} L_{1m} du_x + (\partial/\partial y) \int f_3 h_{1n} L_{1m} du_x]$$

$$+ \sum_n K_{xn}[\int f_1 h_{3n} L_{1m} du_x + (\partial/\partial y) \int f_2 h_{2n} L_{1m} du_x] \tag{4.42}$$

$$\int_{-w}^{w} t_{xm}\{\partial J/\partial x\}dx = -\sum_n K_{zn}[ju_z \int f_1 h_{1n} L_{3m} du_x + (\partial/\partial y) \int f_3 h_{1n} L_{3m} du_x]$$

$$-\sum_n K_{xn} [\int f_1 h_{3n} L_{3m} du_x + (\partial/\partial y) \int f_2 h_{2n} L_{3m} du_x] \tag{4.43}$$

where integration by parts, to place x derivatives onto testing functions, is used to derive (4.43).

4.5.3 Simultaneous Equations for Expansion Coefficients

Substituting into the coupled integral equations and collecting terms,

$$\sum_n K_{zn} M_{zzmn} + \sum_n K_{xn} M_{zxmn} = 0 \tag{4.44a}$$

$$\sum_n K_{zn} M_{xzmn} + \sum_n K_{xn} M_{xxmn} = 0 \tag{4.44b}$$

where m takes values appropriate for each equation (depending upon symmetry of the mode under consideration). Next, exchange partials with respect to y and spectral integrals; understand evaluation at y=0 after taking derivatives of the f functions. Then,

$$M_{zzmn} = \int [-\gamma_c^2 f_1 + j u_z f_3'] h_{1n} L_{1m} du_x \tag{4.45a}$$

$$M_{zxmn} = j u_z \int [f_1 h_{3n} + f_2' h_{2n}] L_{1m} du_x \tag{4.45b}$$

$$M_{xzmn} = - \int [j u_z f_1 + f_3'] h_{1n} L_{3m} du_x \tag{4.45c}$$

$$M_{xxmn} = \int \{k_c^2 f_1 h_{2n} L_{2m} - [f_1 h_{3n} + f_2' h_{2n}] L_{3m}\} du_x \tag{4.45d}$$

where the prime denotes partial differentiation, and where

$$f_1 = (1+R_t)/p_c \tag{4.46a}$$

$$f'_{(2,3)} = -jCu_{x,z} \tag{4.46b}$$

4.5.4 Computational Methods

Techniques used for computation in this case parallel those discussed in section 4.4.2. However, there exists here the additional complication that each matrix element is a double integral instead of a single integral. This is because convenient closed form expressions could not be found for the h_n and L_m functions. Both the inner-nested (x-related) and outer (u_x-related) integrals are therefore done numerically by Simpson's rule. Moreover, due to the unknown nature of matrix elements in the present case, Gaussian quadrature was abandoned in favor of adaptive Simpson's rule for approximation of improper integrals.

4.6 Results

Microstrip propagation modes may be classified into (1) the fundamental, and (2) higher-order modes. The quasi-TEM fundamental mode receives extensive attention in literature on microwave theory; therefore, it is the first to be treated in the present research.

Dispersion characteristics for the fundamental mode on narrow strips are presented by Denlinger [3] and by Itoh and Mittra [20]. These provide data for comparison with results gained by the EFIE method. Figures 10 and 11 show dispersion curves plotted for various methods. On these graphs, "pulse" refers to the pulse function expasion of (4.17) with N as the number of partitions on (0,w). "Entire"

refers to expansion in entire-domain basis functions as in (4.31); NZ and NX are numbers of expansion functions used to represent axial and transverse currents. In contrast with the papers mentioned above, all variables here are given in normalized form: for example, the normalized propagation constant is u_z/k_f. The normalized x coordinate is x/w. Figure 12 shows dispersion characteristics for strips electrically wider than those treated by most workers.

The fundamental mode has a surface current distribution in which the axial current is an even function of x; then by the surface continuity equation, (4.30), transverse currents are odd in x. Therefore, it is only necessary to show currents in the transverse interval (0,w). Figures 13 and 14 show current distributions, for various normalized strip widths, obtained in the axial current approximation. Distributions for pulse function expansion (Figure 13) clearly indicate the well known square root edge-singularity. This edge behavior is analytically included with the expansion in entire-domain basis functions (Figure 14), thereby improving convergence properties of moment method matrix elements. Figure 15 plots the transverse current for various strip widths. Figures 16 and 17 confirm the validity of neglecting transverse currents, as an approximation, on narrow strips. Demonstrated in Figures 18 and 19 are effects of varying the film refractive index while holding other parameters fixed; both expansion methods produce similar results.

Higher-order microstrip modes receive much less attention in the literature than does the fundamental mode. Dispersion curves for the first odd mode are shown in Figure 20; corresponding axial current distributions are given in Figure 21. Figures 22 and 23 give results

for the second even mode. A sample current distribution for the second odd mode is shown in Figure 24. It is noteworthy here that, within the limits of machine accuracy, all computed values of the propagation eigenvalue u_z are purely real.

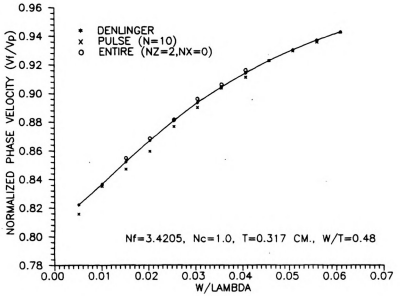

Figure 10. Fundamental mode dispersion characteristics.

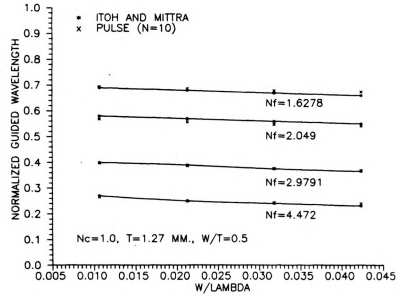

Figure 11. Fundamental mode dispersion characteristics.

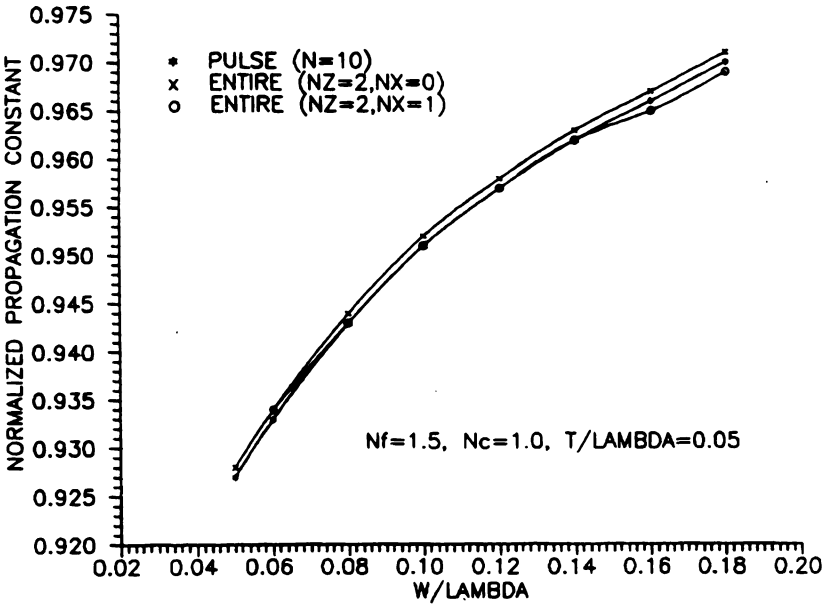

Figure 12. Fundamental mode dispersion characteristics.

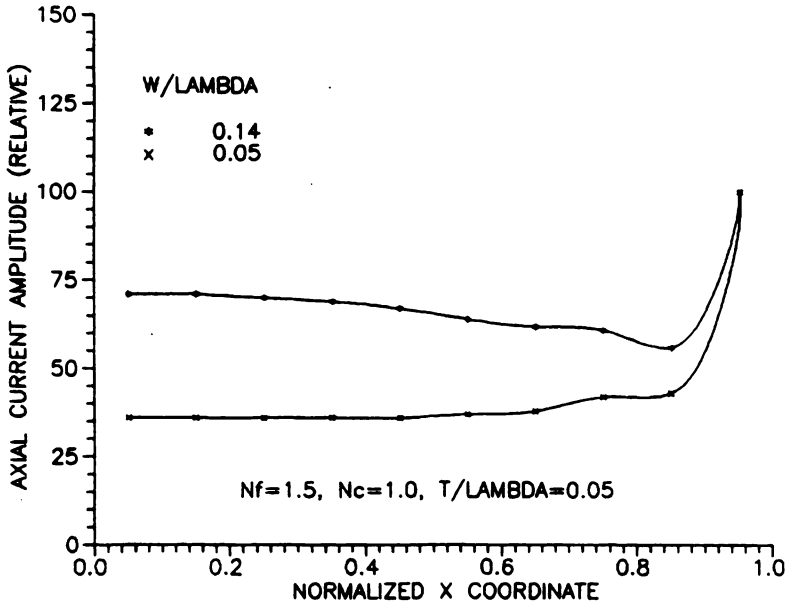

Figure 13. Fundamental mode axial currents.

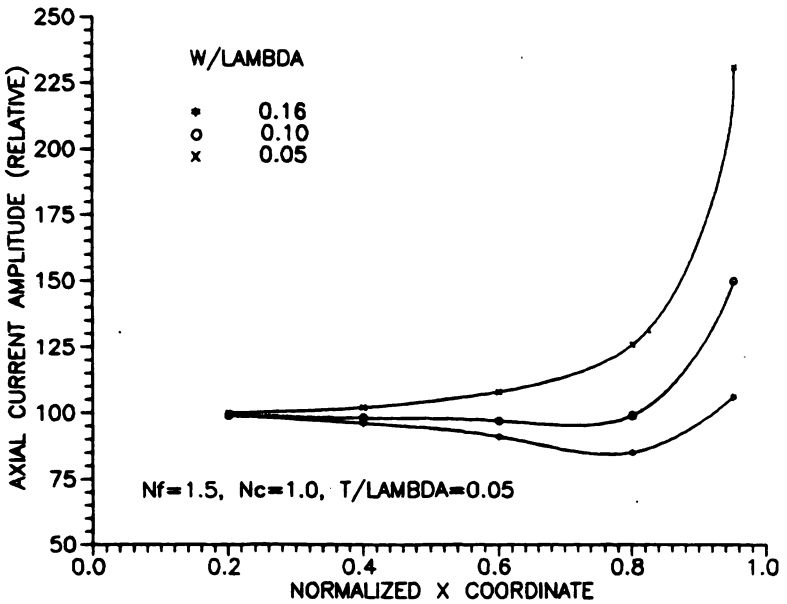

Figure 14. Fundamental mode axial currents.

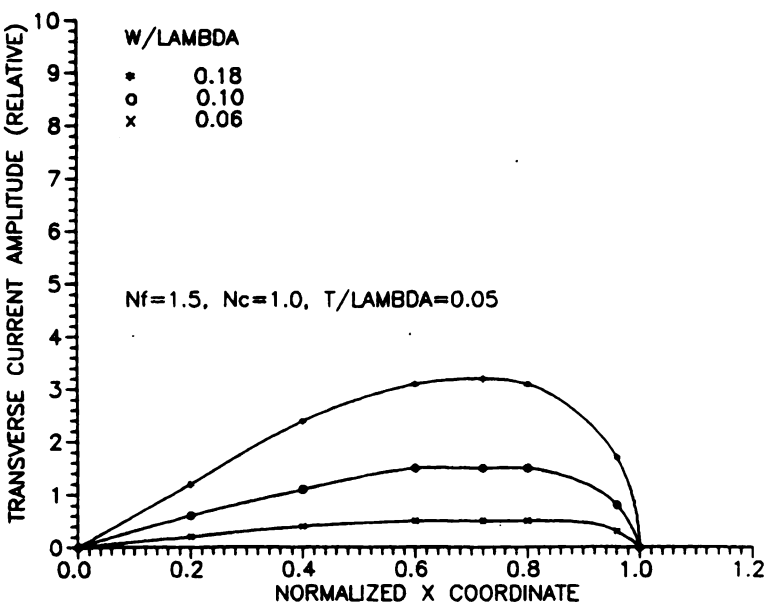

Figure 15. Fundamental mode transverse currents.

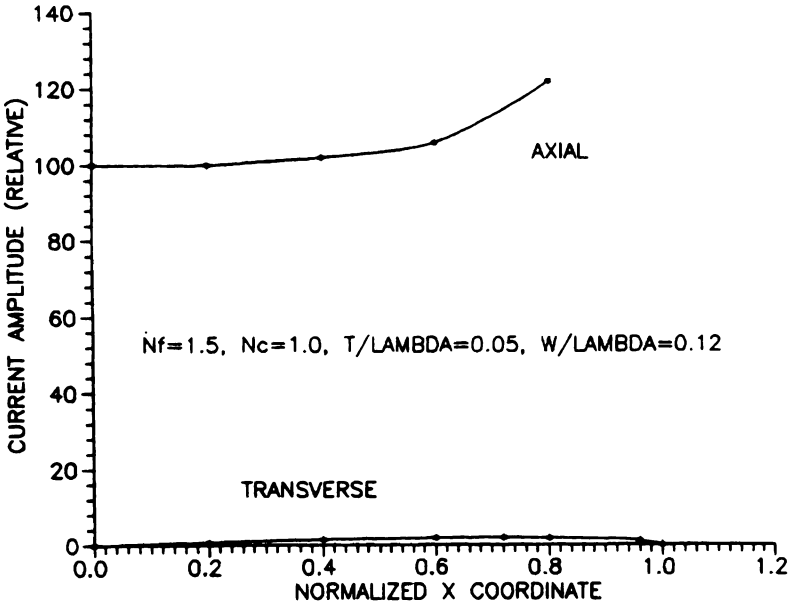

Figure 16. Example of axial and transverse currents.

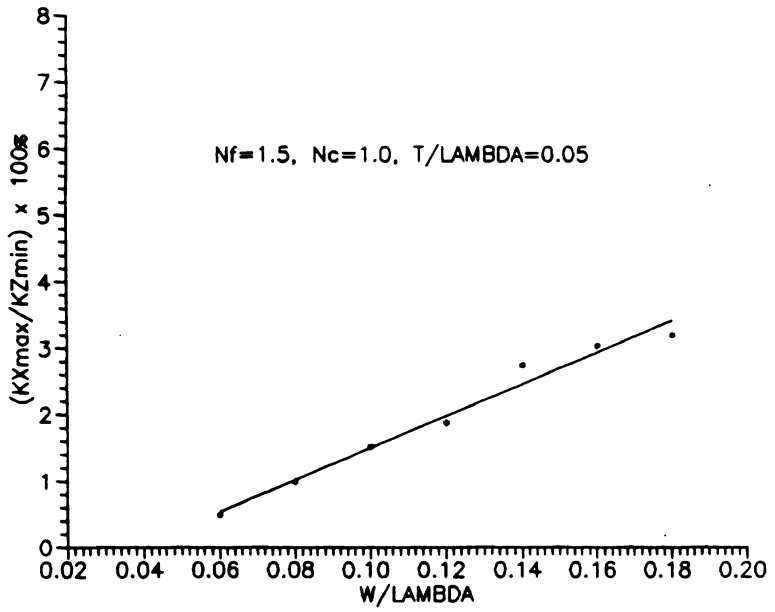

Figure 17. Comparison of axial and transverse current amplitudes.

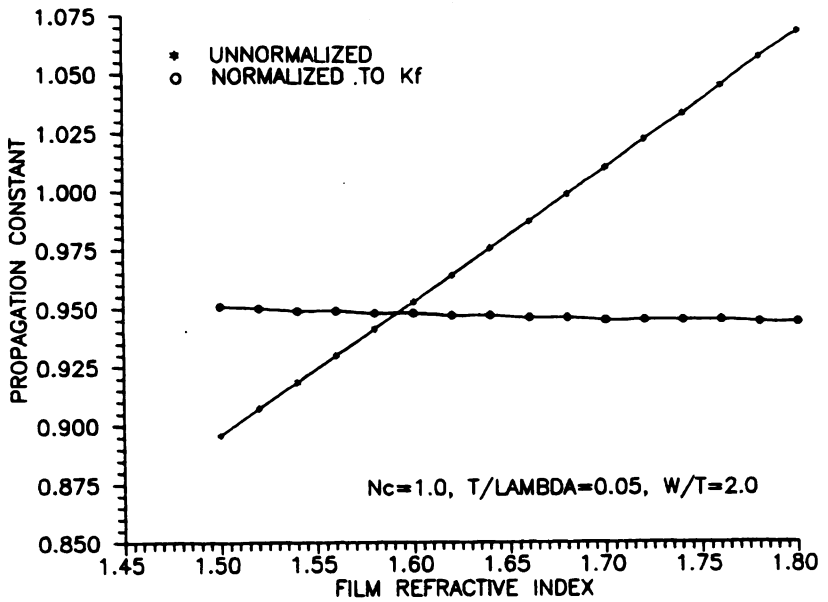

Figure 18. Propagation eigenvalue vs. n_f.

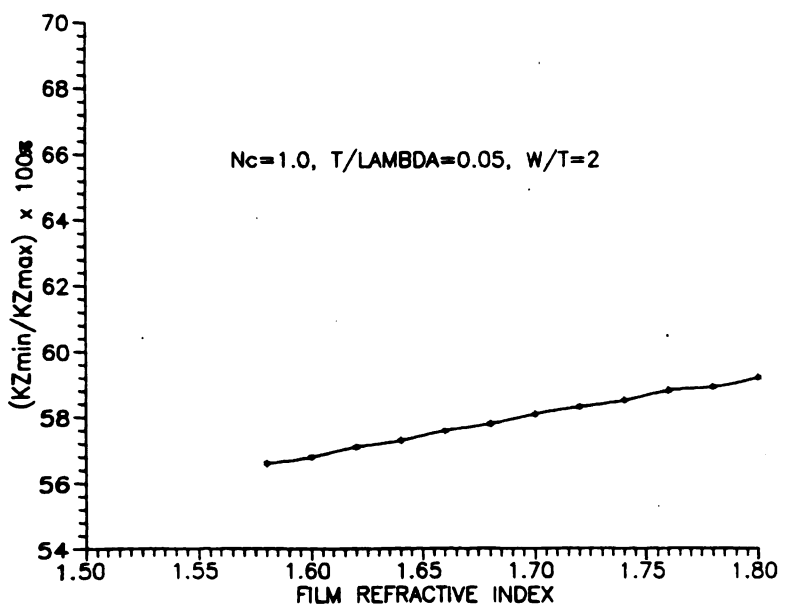

Figure 19. Current amplitude at strip center vs. n_f.

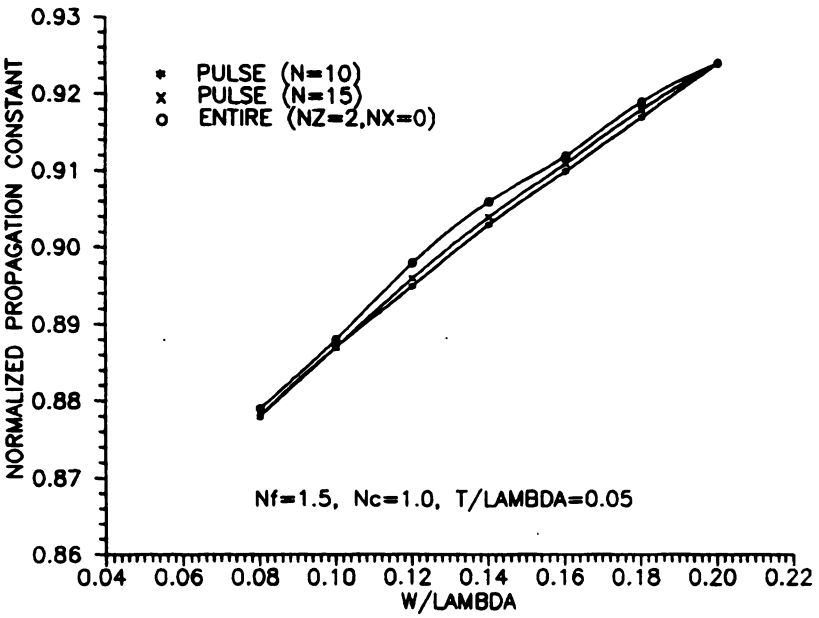

Figure 20. First odd mode dispersion characteristics.

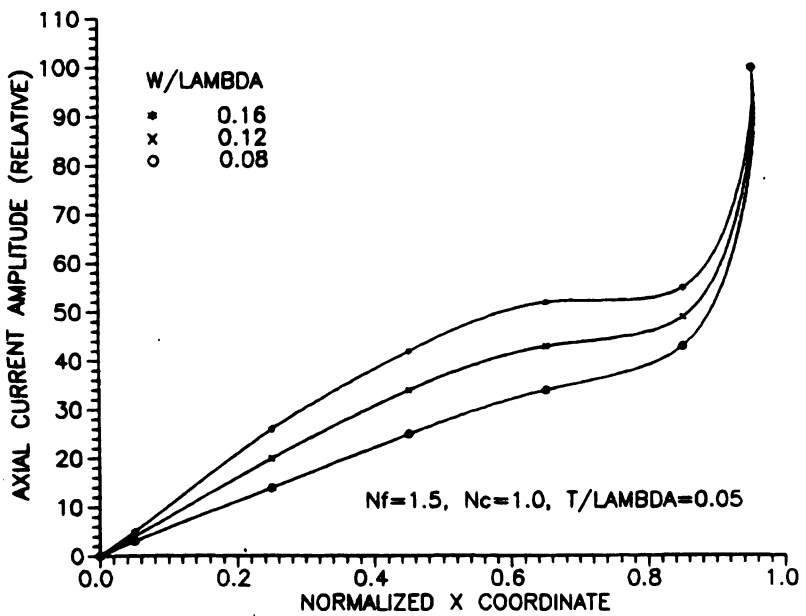

Figure 21. First odd mode axial currents.

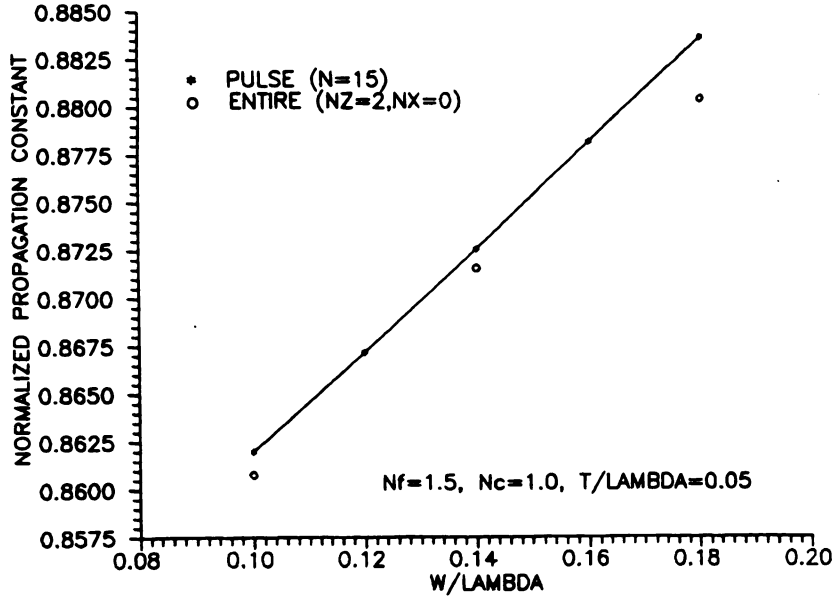

Figure 22. Second even mode dispersion characteristics.

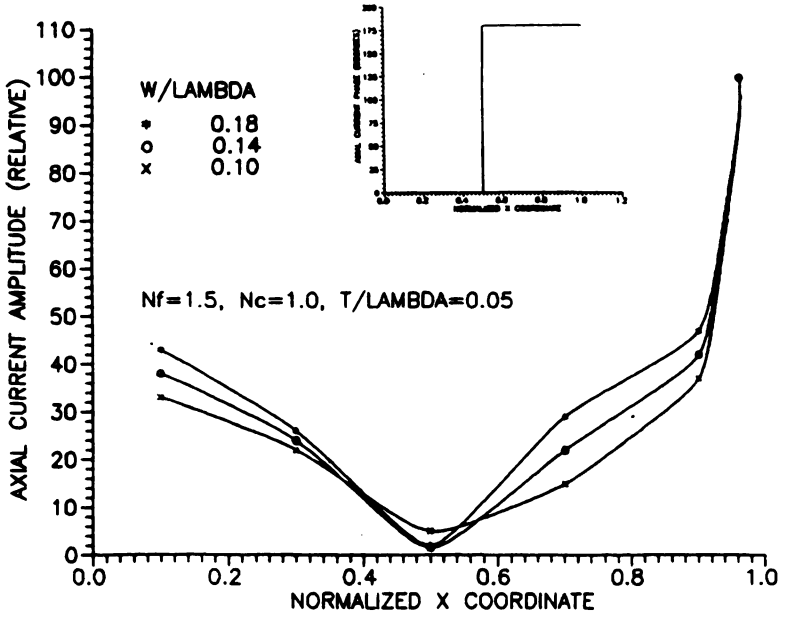

Figure 23. Second even mode axial currents.

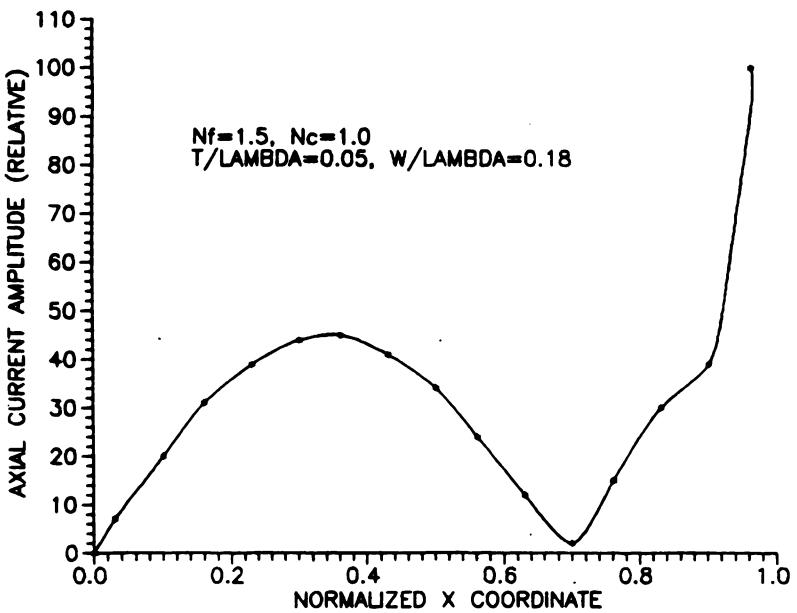

Figure 24. Example of second odd mode axial current.

4.7 Equal Permittivities and the TEM Mode

As in section 2.8, consider the special case of $N_{fc}=1$. The EFIE of section 4.4,

$$\int_{-w}^{w}[-\gamma_c^2(g_p+g_{rt})-u_z^2(\partial g_{rc}/\partial y)]k_z dx' = 0 \qquad (4.47)$$

reduces to

$$\gamma_c^2 \int_{-w}^{w}(g_p+g_{rt})k_z dx' = 0 \qquad (4.48)$$

since coupling coefficient C vanishes. The readily apparent solution to this equation is to have $u_z=k_c$; this is, of course, the expected eigenvalue for the TEM mode of an ordinary two-conductor transmission line embedded in a homogeneous dielectric having refractive index n_c.

4.8 Conclusion

Discrete microstrip modes are quantified in this chapter as natural solutions of the transform-domain EFIE. The integral equation is solved by moment method, implementing both subsectional and entire-domain basis functions. Results are displayed for fundamental and higher-order modes. All modes recovered are purely propagating, with no evidence of leakage [32,33] phenomena (i.e., u_z not complex). However, it is anticipated that further study will reveal leaky modes in some parameter regime [21].

CHAPTER V

THE CONTINUOUS SPECTRUM

5.1 Introduction

In Chapter 3 it is shown that forced EFIE solutions form the microstrip's continuous spectrum. The forcing function is an impressed electric field, depending upon transform variable u_z at points along the u_z-plane branch cut. Solutions of the forced EFIE, equation (3.3), are sought in the present chapter; these are spectral component contributions to microstrip radiation mode currents.

5.2 Microstrip Excitation

Assume that microstrip excitation is provided by a monopole antenna emergent from the substrate and radiating into the film under the strip (as in Figure 25). Calculation of electric fields impressed by this radiating element requires the Green's function for vertical sources embedded in the film; this is derived in section 5.3.

5.3 Green's Function for Vertical Current in Film

The analysis for vertical sources in the film layer is simple, mainly because the y-component of Hertz potential is present exclusively. Boundary conditions for potential are therefore simplified greatly, compared with Chapter 2. Using results from section 2.5.1, case (a), boundary conditions at y=0 are

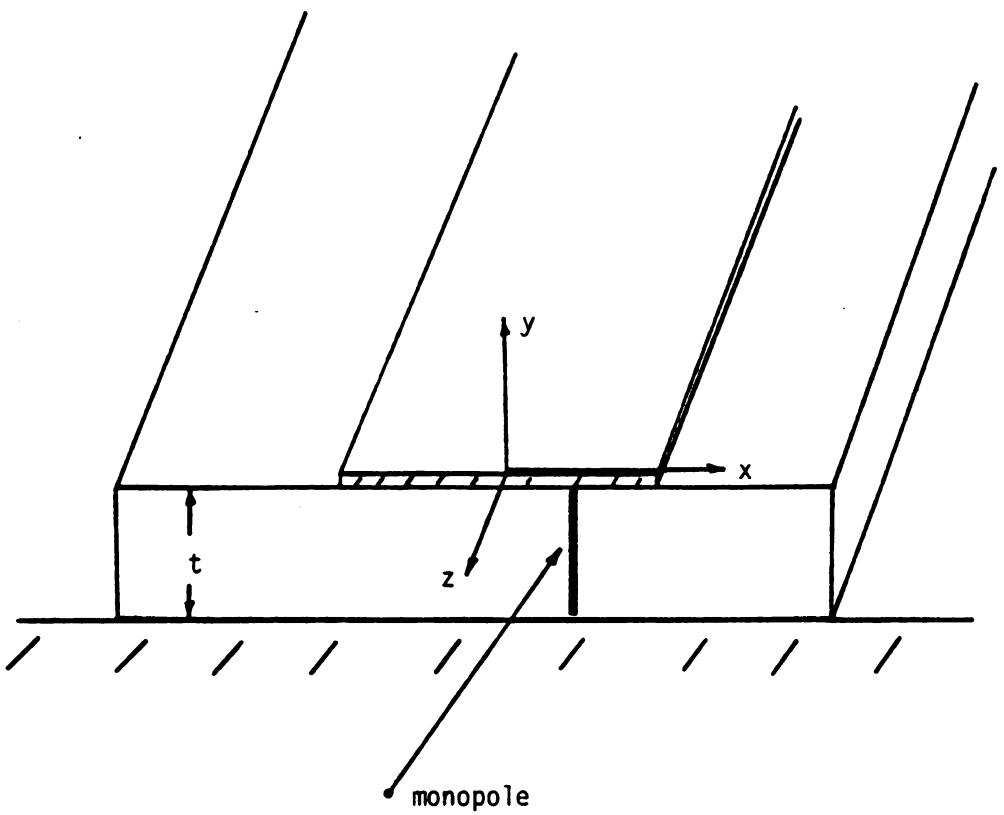

Figure 25. Microstrip excitation.

$$Z_{fy} = N_{cf} Z_{cy} \tag{5.1a}$$

$$(\partial/\partial y)[Z_{cy} - Z_{fy}] = 0 \tag{5.1b}$$

where $N_{cf}=(n_c/n_f)^2$. Using results from section 2.5.2, case (a), the condition at y=-t is

$$\partial Z_{fy}/\partial y = 0 \tag{5.2}$$

Paralleling section 2.6, but with some modification for sources in the film, integral representations for potential are constructed:

$$Z_{fy} = (1/A_0) \iint \exp(j\vec{L}\cdot\vec{r})\{V + W_{f1}\exp(-p_f y) + W_{f2}\exp(p_f y)\}d^2L \tag{5.3a}$$

$$Z_{cy} = (1/A_0) \iint \exp(j\vec{L}\cdot\vec{r})\{W_c \exp(-p_c y)\}d^2L \tag{5.3b}$$

where

$$V = \int_V [J_y(\vec{r}')/2p_f A_f]\exp(-j\vec{L}\cdot\vec{r}')\exp(-p_f|y-y'|)dV' \tag{5.4}$$

and $A_f=j\omega\varepsilon_f$. Substituting equations (5.3) into boundary conditions (5.1) and (5.2) gives three algebraic equations for unknown spectral amplitudes W_{f1}, W_{f2}, and W_c. The unknown of interest is W_c, as it gives fields in the cover (where the strip is located at y=0+). Solving for W_c,

$$W_c = \int_V \frac{J_y(\vec{r}')\exp(-j\vec{L}\cdot\vec{r}')\cosh[p_f(y'+t)]}{A_f[N_{cf}p_f\sinh(p_f t)+p_c\cosh(p_f t)]}\,dV' \qquad (5.5)$$

Z_{cy} is found by back-substitution into equation (5.3b).

Assuming J_y to be the uniform, unit-strength, elemental line current given by $J_y=\delta(x-x_m,z-z_m)$ for $-t<y<0$, Z_{cy} transforms axially to:

$$z_{cy} = \frac{\exp(-ju_z z_m)}{2\pi A_f}\int \frac{\exp[ju_x(x-x_m)]\exp(-p_c y)}{p_f[N_{cf}p_f+p_c\coth(p_f t)]}\,du_x \qquad (5.6)$$

Electric fields are given in terms of Hertz potential in equation (2.2a). Anticipating future focus on the dominant axial component of current, only the gradient of divergence term contributes to e_z; therefore,

$$e_z = ju_z\partial Z_{cy}/\partial y = \frac{u_z\exp(-ju_z z_m)}{j2\pi A_f}\int \frac{\exp[ju_x(x-x_m)]\exp(-p_c y)}{(p_f/p_c)[N_{cf}p_f+p_c\coth(p_f t)]}\,du_x \qquad (5.7)$$

5.4 Dominant Axial Current Approximation

Assume that, for narrow microstrip line, the only significant component of current is axial. This approximation is consistent with Chapter 4, where it proves adequate for discrete modes propagating on narrow strips. The axial-transform-domain inhomogeneous EFIE arises from equation (3.3), and is

$$k_c^2 \int_{-w}^{w} (g_p+g_{rt}) k_z dx' + j u_z \tilde{\nabla} \cdot \int_{-w}^{w} \bar{\bar{g}} \cdot \vec{k} \, dx' = -A_c \hat{z} \cdot \vec{e}^i(\vec{\rho}, u_z) \tag{5.8}$$

with evaluation $y=y'=0$ understood; the equation holds for all points u_z along the branch cut, as discussed in section 3.4.

5.5 Wavenumber Parameters Along Branch Cut

Consider the wavenumber parameters p_c and p_f. They are each of the general form

$$p = (u_x^2+u_z^2-k^2)^{1/2} = [(u_x+j\gamma)(u_x-j\gamma)]^{1/2} \tag{5.9}$$

where $\gamma = [(u_z-k)(u_z+k)]^{1/2}$. As established in section 3.4 the complex u_z plane features branch points $\pm k$, with associated hyperbolic cuts, defining γ as a single-valued function whose argument depends greatly upon the location of u_z relative to the cut. For example, as u_z is varied around $-k$ from one side of the cut to the other, the angle of γ changes abruptly by 180^o. The location of u_z relative to the cut (see Figure 26) therefore profoundly impacts wavenumber parameter evaluation. Branch points in the complex u_x plane occur at $\pm j\gamma$. As $\mathrm{Re}\{\gamma\}$ is limitingly small, $\mathrm{Im}\{j\gamma\}$ is correspondingly small; and, as in Figure 27, u_x-plane branch point locations depend upon u_z relative to its cut. For $|u_{xr}|>|\gamma_i|$, $\arg\{p\}$ is essentially zero. For $|u_{xr}|<|\gamma_i|$, $\arg\{p\}$ is 90^o for $u_z=u_{z1}$ and is -90^o for $u_z=u_{z2}$. Hence, values of p on alternate sides of the u_z-plane cut are complex conjugates. Since equation (5.6) is even in p_f, k_f related cuts are not

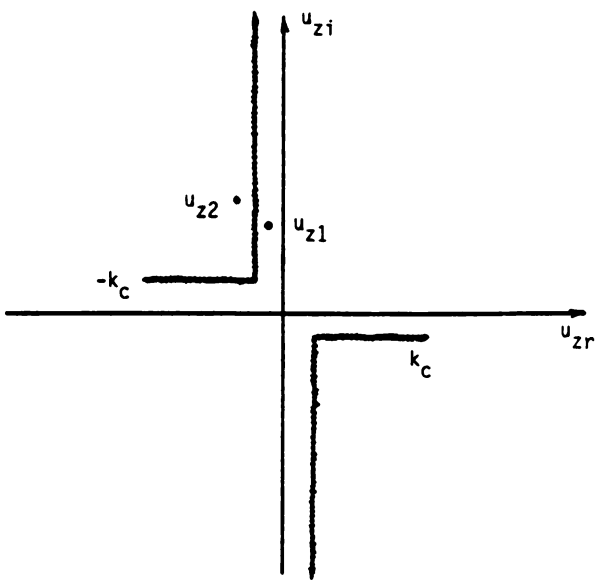

Figure 26. Locations of u_z relative to branch cut.

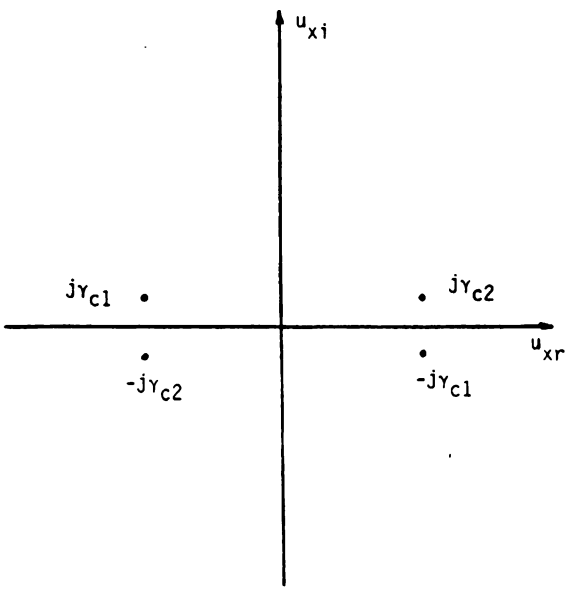

Figure 27. Branch points in complex u_x plane.

implicated and only k_c related cuts in the complex u_z-plane matter. Finally compute p_c from

$$p_c = \begin{cases} [u_x^2-Q]^{1/2} \text{ if } |u_x|>|Q|^{1/2} \\ +j[Q-u_x^2]^{1/2} \text{ if } |u_x|<|Q|^{1/2},\ u_z=u_{z1} \\ -j[Q-u_x^2]^{1/2} \text{ if } |u_x|<|Q|^{1/2},\ u_z=u_{z2} \end{cases} \tag{5.10}$$

where $Q=k_c^2-u_z^2$.

5.6 Moment Method Solution of Spectral EFIE

EFIE numerical solution takes place pointwise along the u_z-plane branch cut. Explicitly, the equation to be solved is:

$$\int_{-w}^{w}\int U\exp[ju_x(x-x')]k_z du_x dx' = -2\pi jk_c\hat{z}\cdot e^i(x,0,u_z) \tag{5.11}$$

where

$$U = [-\gamma_c^2+u_z^2p_c(N_{fc}-1)/Z_e]/Z_h \tag{5.12}$$

In general it is hard to solve Fredholm equations of the first kind, such as (5.11). Since the first-kind equation doesn't lead to iterative solutions, moment method is exploited here to gain preliminary results. Galerkin's method with pulse functions for expansion and testing (see section 4.4.1) gives

$$\sum_n K_{zn} \int UT^2 \exp[ju_x(x_m-x_n)]du_x =$$

$$\frac{ju_z \exp(-ju_z z_m)}{2N_{fc}} \int \frac{p_c T \exp[ju_x(x_m-x_m)]}{p_f[N_{cf}p_f+p_c \coth(p_f t)]} du_x \qquad (5.13)$$

where $T=[\sin(u_x h)]/u_x$.

5.7 Results

Figure 28 shows solutions of (5.13) for various values of parameter u_z. The equation is solved for the strip dimensions and physical parameters as indicated in the figure; for simplicity the excitation monopole is located at ($x_m=0, z_m=0$), the geometrical strip center. These functions are individual contributions to the current of the microstrip continuous spectrum.

Note the behavior of the spectral components as u_z moves out on the branch cut: the currents increase, pass what appears to be resonant level, and finally begin to oscillate while decreasing in amplitude. Indeed, examining the u_z dependence of each term in equation (5.13) does lead one to expect the amplitude decrease. The resonant phenomenon is probably associated with the combined effects of incident and reflected electric fields. At values of u_z well past the "resonance", the impressed field is primarily responsible for driving the currents; therefore, it is expected that for large u_z the currents will oscillate in a pattern resembling e^{j}.

In addition to the u_z values given in Figure 28, which all fall on the imaginary-axis part of the branch cut, u_z values along the real-axis section of the cut were investigated. The continuous

spectrum functions associated with the latter u_z are found to resemble curves 1 and 2 of Figure 28. These additional curves are omitted from the graph to avoid confusion.

Finally, one senses a disadvantage of moment method solution to this problem: very fine partitioning would be needed to continue this solution process ad infinitum. Perhaps, for future work, iterative methods of solution (for example [22]) are worth investigating.

5.8 Conclusion

Microstrip modes belonging to the continuous spectrum are quantified in this chapter as forced solutions of the transform-domain EFIE. The problem is solved for fields impressed by vertical currents under the strip; furthermore, transverse currents are neglected for simplicity. Numerical results, gained by the moment method, are presented. It is important to note that the functions shown do not represent the final solution to the continuous spectrum problem; rather, the solution process is just beginning. Once a feasibly quick method of solution for equation (5.8) is developed, it remains to substitute the spectral components into (3.12).

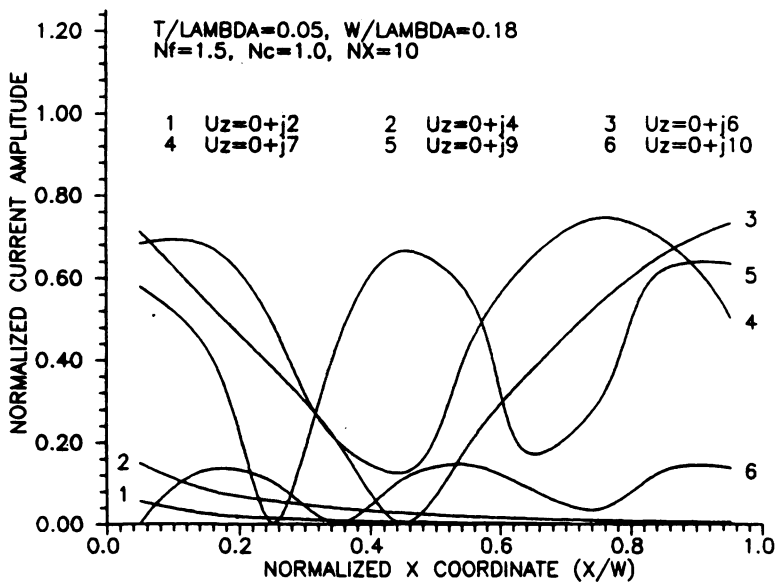

Figure 28. Solutions of the forced EFIE.

CHAPTER VI

COUPLING BETWEEN ADJACENT MICROSTRIP LINES

6.1 Introduction

Coupling phenomena are of great importance in the design of high-speed integrated circuits. These effects are undesirable in some circuits (e.g. crosstalk in communication hardware); in others the design itself depends on their existence (e.g. microwave couplers).

Microstrip coupling problems are treated by various approximate methods in the literature. For example, [23] uses a "directly-coupled parallel-plate ideal waveguide model" with quasi-static parameters. The so-called LSE model of [24] is another quasi-TEM approach.

The transform-domain EFIE provides a basis for studying coupling phenomena in axially-uniform multi-strip systems. The problem is formulated in detail here, and preliminary numerical results are obtained for a simple case.

6.2 Geometry of Multi-Strip System

Consider N parallel microstrip lines as shown in Figure 29. Let C_n denote the n'th microstrip periphery contour, and $\vec{k}_n$ the current density on the n'th strip. Unit vector $\hat{t}_m$ is tangent everywhere to the m'th strip surface. As in previous chapters, the strips are integrated over a dielectric film layer of thickness t.

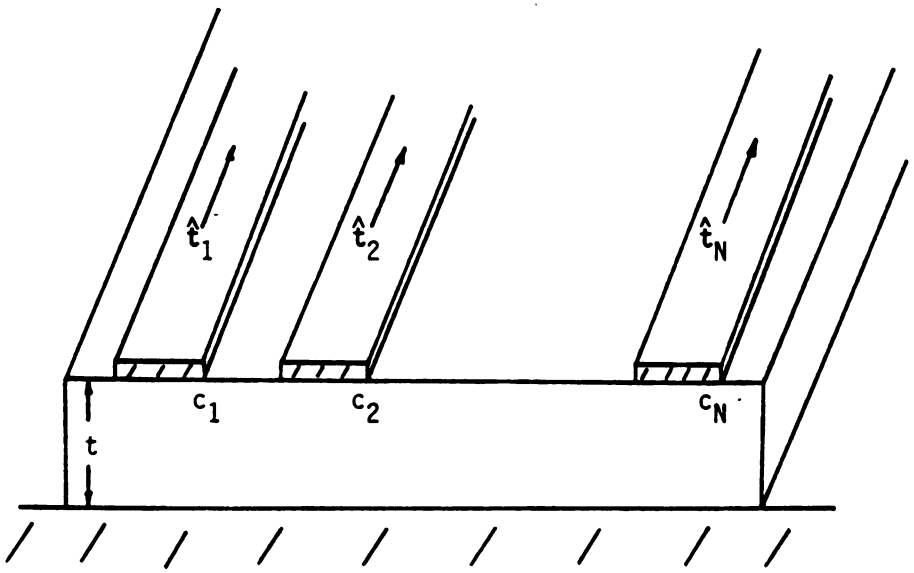

Figure 29. Parallel microstrips.

6.3 Transform-domain EFIE for Propagation Modes

Formulation of this problem parallels earlier chapters. However, the metallic cross-section over which the EFIE is enforced must be collectively the set of strip cross-sections. Moreover, the electric Green's dyad $\bar{\bar{g}}_e$ proves valuable in formulation and early theoretical stages of the present problem. Based on the tangential electric field boundary condition, formulate the EFIE as the system

$$\hat{t}_m \cdot \sum_{n=1}^{N} \int_{C_n} \bar{\bar{g}}_e(\vec{\rho},\vec{\rho}') \cdot \vec{k}_n(\vec{\rho}',u_z)dl' = -A_c \hat{t}_m \cdot \vec{e}^i(\vec{\rho},u_z) \qquad (6.1)$$

which holds for all $\vec{\rho}$ on C_m; m=1,2,3,...,N. Again, note $A_c=j\omega\varepsilon_c$.

System propagation modes are characterized by coupled currents sharing u_z-plane simple poles. Furthermore, it is important to note that propagation-mode coupling becomes significant only when the isolated microstrip mode propagation constants are nearly equal.

By arguments analogous to those for the isolated microstrip, when u_z is the propagation-mode eigenvalue associated with the simple-pole u_z-plane singularity, the natural eigenmode currents satisfy a system of homogeneous transform-domain integral equations:

$$\hat{t}_m \cdot \sum_{n=1}^{N} \int_{C_n} \bar{\bar{g}}_e(\vec{\rho},\vec{\rho}') \cdot \vec{k}_n(\vec{\rho}')dl' = 0 \qquad (6.2)$$

holding for all $\vec{\rho}$ on C_m; m=1,2,3,...,N. Note that the electric Green's dyad depends implicitly upon u_z.

6.4 Testing Operation

In equation (6.2), in place of the simple pre-dot operation with $\hat{t}_m$, apply the testing operator

$$\int_{C_m} dl\ \vec{k}_{m0}(\vec{\rho})\cdot$$

for m=1,...,N. Embedded in this operator is $\vec{k}_{m0}$, the propagation-mode current of the m'th strip (when isolated from other strips). Since $\vec{k}_{m0}$ is tangent everywhere to strip surfaces, this testing operation is a suitable replacement for the original operation; its motivation becomes apparent in the following section. After testing,

$$\int_{C_m} dl\ \vec{k}_{m0}(\vec{\rho})\cdot \sum_{n=1}^{N} \int_{C_n} \bar{\bar{g}}_e(\vec{\rho},\vec{\rho}')\cdot\vec{k}_n(\vec{\rho}')dl' = 0 \qquad (6.3)$$

for m=1,...,N.

6.5 Approximations for Loose Coupling

In weak, nearly-degenerate coupling, propagation constant u_z remains close to the (approximately equal) values u_{zn0} of the isolated strips. For the electric Green's dyad, take the leading two terms in a Taylor's series expansion about u_{zn0}:

$$\bar{\bar{g}}_e = \bar{\bar{g}}_e\Big|_{u_{zn0}} + (u_z-u_{zn0})(d\bar{\bar{g}}_e/du_z)\Big|_{u_{zn0}} = \bar{\bar{g}}_{e0}+(u_z-u_{zn0})\bar{\bar{g}}_{e0}' \qquad (6.4)$$

Substitute into the EFIE system, (6.3), and exploit the reciprocal

property [25] of the electric Green's dyad. Retain only leading, non-vanishing terms:

$$\int_{C_m} dl' \vec{k}_m(\vec{\rho}') \cdot \int_{C_m} \bar{\bar{g}}_{e0}'(\vec{\rho}', \vec{\rho})(u_z - u_{zm0}) \cdot \vec{k}_{m0}(\vec{\rho}) dl +$$

$$\sum_n \int_{C_n} dl' \vec{k}_n(\vec{\rho}') \cdot \int_{C_m} \bar{\bar{g}}_{e0}(\vec{\rho}', \vec{\rho}) \cdot \vec{k}_{m0}(\vec{\rho}) dl = 0 \qquad (6.5)$$

where the defining EFIE for isolated eigenmode current $\vec{k}_{m0}$ has been exploited, and the summation now excludes n=m.

As a perturbation approximation, assume $\vec{k}_n = a_n \vec{k}_{n0}$ where a_n is a constant. That is, the functional form of this approximation resembles an isolated strip current: only the amplitude is allowed to differ. Again invoking Green's dyad reciprocity gives

$$a_m \bar{c}_{mm}(u_z - u_{zm0}) + \sum_n c_{mn} a_n = 0; \; m=1,\ldots,N \qquad (6.6)$$

where

$$\bar{c}_{mm} = \int_{C_m} dl \int_{C_m} dl' \; \vec{k}_{m0}(\vec{\rho}) \cdot \bar{\bar{g}}_{e0}'(\vec{\rho}, \vec{\rho}') \cdot \vec{k}_{m0}(\vec{\rho}') \qquad (6.7a)$$

$$c_{mn} = \int_{C_m} dl \; \vec{k}_{m0}(\vec{\rho}) \cdot \int_{C_n} \bar{\bar{g}}_{e0}(\vec{\rho}, \vec{\rho}') \cdot \vec{k}_{n0}(\vec{\rho}') dl' \qquad (6.7b)$$

and the summation over n excludes n=m. Equation (6.6) is an algebraic system for the unknown u_z. Coefficients (6.7) dictate the location of

u_z relative to the nearly identical values of u_{zm0}.

6.6 Illustration For Two Strips

Letting N=2 and solving algebraic system (6.6) for u_z gives

$$u_z = Q_1 \pm Q_2 \tag{6.8}$$

where $Q_1=(u_{z10}+u_{z20})/2$ is the average of the isolated strip propagation constants and

$$Q_2 = [Q_3^2+Q_4^2]^{1/2} \tag{6.9a}$$

$$Q_3 = (u_{z10}-u_{z20})/2 \tag{6.9b}$$

$$Q_4 = (c_{12}c_{21})/(\bar{c}_{11}\bar{c}_{22}) \tag{6.9c}$$

Thus two shifted, coupled-mode eigenvalues result when N=2; they are symmetrically placed about the average of the isolated strip values.

6.7 Overlap Integral For Coupling Coefficient

Equation (6.7b) is converted to a more useful form by recognizing

$$\int_{C_n} \bar{\bar{g}}_{e0}(\vec{\rho},\vec{\rho}')\cdot\vec{k}_{n0}(\vec{\rho}')dl' = A_c\vec{e}_{n0}(\vec{\rho}) \tag{6.8}$$

where $\vec{e}_{n0}$ is the electric field maintained everywhere by surface currents on the n'th strip. Substituting into (6.7b),

$$c_{mn} = A_c \int_{C_m} \vec{k}_{m0}(\vec{\rho}) \cdot \vec{e}_{n0}(\vec{\rho}) dl \qquad (6.9)$$

which is explicitly an overlap integral, providing a physical picture in which currents on the m'th strip link with fields of the n'th strip. Equation (6.9) is also computationally better than (6.7b), because e_{n0} is easily written in terms of the Hertz potential Green's dyad:

$$\vec{e}_{n0}(\vec{\rho}) = (1/A_c)\{k_c^2 + \tilde{\nabla}\tilde{\nabla}\cdot\} \int_{C_n} \bar{\bar{g}}(\vec{\rho},\vec{\rho}') \cdot \vec{k}_{n0}(\vec{\rho}') dl' \qquad (6.10)$$

The overlap integral formulation is physically significant because, referring to equations (6.6) and (6.7), the amount of overlap bears directly upon the strength of coupling between any two microstrip lines. The remainder of this chapter is therefore devoted to overlap integrals for the fundamental modes of thin and narrow strips.

6.8 Overlap Integral For Thin, Narrow Strips

Let $x=p_i$ be the center location of the i'th strip; the strip extends over (p_i-w_i, p_i+w_i). Invoke the dominant axial current approximation by neglecting transverse currents on narrow strips. Then for thin microstrip lines, (6.9) becomes

$$c_{mn} = A_c \int_{(p_m-w_m)}^{(p_m+w_m)} k_{m0}(x)[\hat{z}\cdot\vec{e}_{n0}(x)]dx \qquad (6.11a)$$

where

$$\hat{z}\cdot\vec{e}_{n0}(x) = (1/2\pi A_c)\int_{(p_n-w_n)}^{(p_n+w_n)} k_{n0}(x')\int U\exp[u_x(x-x')]du_x dx' \tag{6.11b}$$

and

$$U = [-\gamma_c^2+u_z^2 p_c(N_{fc}-1)/Z_e]/Z_h \tag{6.11c}$$

Note that equation (6.11c) has $u_z=u_{zn0}$.

To approximate fundamental mode coupling, let the current on the i'th strip be represented by the leading term of equation (4.31a). That is, take

$$k_{i0}(x) = a_i/\{1-[(x-p_i)/w_i]^2\}^{1/2} \tag{6.12}$$

for x in (p_i-w_i, p_i+w_i), and substitute into (6.11a) and (6.11b).

Some preliminary numerical results, obtained under the approximations of this section, are given next.

6.9 Results and Conclusion

Figure 30 depicts an example of overlap integral behavior vs. separation between two parallel microstrips. The overlap integral is done numerically by Simpson's rule. Physical parameters chosen for

the example are given in the text of the figure. A best-fit exponential curve appears along with the data points. Coupling decreases rapidly with increasing distance in this case.

These preliminary results are given for illustration; obviously many other cases await treatment (e.g., effect of changing strip and film dimensions, effect of altering medium parameters, effect of including more terms in the current expansion, and coupling between higher-order modes).

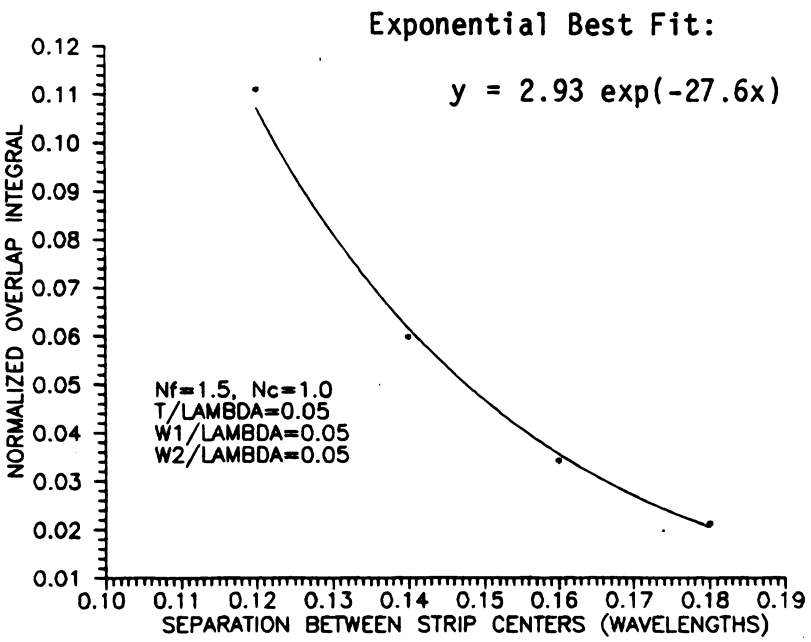

Figure 30. Overlap integral vs. strip separation.

CHAPTER VII

CONCLUSION AND RECOMMENDATION

Electromagnetic waves and their interactions in integrated circuits form a challenging area for investigation. The EFIE approach departs from other, less cogent methods of approximate analysis; it is appealing due to its simplicity and conceptual exactness. It predicts the existence of both discrete and continuous microstrip spectra, and permits their numerical calculation. In addition, it facilitates the study of important electromagnetic coupling phenomena. Nevertheless, because of the high computational demands of even simple problems, it is doubtful that the EFIE will soon supplant faster methods for design work.

Chapter 2 of this dissertation outlines in somewhat general form the electromagnetic theory relevant to high-speed integrated circuits. This formulation applies not only to infinite strips, but also to various patch antennas and integrated devices composed of finite strips. The successful application of this theory to the circular patch, with initial emphasis on the low-order resonant modes, is currently underway.

The rigorous identification of discrete and continuous microstrip eigenvalue spectra via complex plane analysis, as presented in Chapter 3, is believed to be new. Some observations made in that chapter are probably fundamental to knowledge of the microstrip as an open-

boundary waveguiding structure. That chapter also provides a crucial link between the theory and its application, viz., that of associating the homogeneous IE with discrete modes and the forced IE with the continuous spectrum.

Moment methods, attempted with various expansion functions, perform well in solving the homogeneous microstrip IE of Chapter 4. Fundamental mode eigenvalues match those published by other authors, thereby providing solid validation for the EFIE approach. Higher-order mode solutions are easily generated once their determinantal zeros are located; however, these zeros are found only by somewhat fortuitous searching. Certainly, with continued effort, more higher-order modes will be located; research should be encouraged to catalog these modes completely.

The continuous spectrum is a topic on which, to date, only sparse information is available. Chapter 5 brings forward some preliminary results for consideration. Forthcoming research, perhaps using combinations of different numerical methods, will perforce shed much light on this new area.

Coupling between parallel microstrips is addressed in Chapter 6. Of course, much more work remains in this area. Other topics of interest (besides those already mentioned in section 6.9) include coupling between nonparallel strips, and coupling from strips to adjacent printed antennas.

APPENDICES

APPENDIX A

APPENDIX A

ACCURATE EVALUATION OF SOMMERFELD INTEGRALS USING THE FAST FOURIER TRANSFORM

An approach to real-axis numerical evaluation of Sommerfeld-type [26] integrals is advanced in this appendix. The method combines the Fast Fourier Transform (FFT) algorithm with Simpson's rule. References such as [27,28,29] discuss the FFT for periodic functions only. A principal advantage is that a single FFT call gives many sample values of an integral with respect to an integrand parameter. Such samples could be immediate goals, as when the parameter is a spatial coordinate variable. In other cases, the Sommerfeld integral is a Green's function occurring in a spatial integral: here, too, sample values are desired.

To estimate an integral such as

$$I = \int_a^b f(t)dt$$

partition [a,b] into N subintervals $[t_i,t_{i+1}]$ with $t_i=a+hi$, $i=0,1,2,\ldots,N-1$. The step size h is (b-a)/N. Figure 31 outlines integration rules [30], provided f(t) is sufficiently smooth. Rule names, corresponding to numbers in the figure, are: (1) rectangular, (2) trapezoidal, (3) corrected trapezoidal, and (4) Simpson's. (Note: N is even for Simpson's rule.) Observe that rectangular and corrected

Integration Rule	Error
1. $h \sum_{i=0}^{N-1} f(t_i)$	$h(b-a)f'(\eta)/2$
2. $h \left[\frac{f(a) + f(b)}{2} + \sum_{i=1}^{N-1} f(t_i) \right]$	$-h^2(b-a)f''(\eta)/12$
3. $h \left[\frac{f(a) + f(b)}{2} + \sum_{i=1}^{N-1} f(t_i) \right] + \frac{h^2}{12} [f'(a) - f'(b)]$	$h^4(b-a)f^{(iv)}(\eta)/720$
4. $\frac{h}{3} [f(a) + 4f(t_1) + 2f(t_2) + \ldots + f(b)]$	$-h^4(b-a)f^{(iv)}(\eta)/180$

Figure 31. Numerical integration rules.

trapezoidal rules are identical for integrands periodic on [a,b], since f(a)=f(b) and f'(a)=f'(b). Therefore, a rectangular rule approach to integrating periodic functions really gives corrected trapezoidal rule accuracy.

The FFT algorithm computes the discrete Fourier transform (DFT)

$$S_{k+1} = \sum_{n=0}^{N-1} A_{n+1}\exp(j2\pi kn/N); \quad k=0,1,2,\ldots,N-1$$

of the sequence $A_1,\ldots,A_N$; this is viewed as numerical integration of

$$I(x) = \int_0^T g(t)\exp(jxt)dt$$

as follows. A change of variables transforms the integration limits to span $[0,2\pi]$. Partition this new interval into N equal segments. By rectangular rule,

$$I(x_k) = h \sum_{n=0}^{N-1} g(nh)\exp(j2\pi nk/N),$$

where $h=T/N$ and $x_k=2\pi k/T$. That is $I(x_k)=hS_{k+1}$, where $A_{n+1}=g(nh)$. Observe again that for g(t) periodic on [0,T] the above scheme is corrected trapezoidal rule; however, if g(t) is aperiodic the method is only rectangular rule. In this instance the simple step of letting $A_1=g(0)+g(hN)$, $A_2=4g(h)$, $A_3=2g(2h)$, $A_4=4g(3h)$, ..., conforms to Simpson's rule within a factor of h/3.

To show the improvement, consider the following example. Let $g(t)=\exp(-t^2/2)$, which is proportional to its own transform. Truncation at $T=2\pi$ is adequate with $N=2^{10}$. Direct FFT with unweighted integrand sample values (i.e., rectangular rule) produces an answer correct to one significant figure. The Simpson's rule scheme gives 13 digit accuracy according to [31].

The error introduced by truncating an improper integral having infinite upper limit is bounded by proper choice of T, the stopping point of numerical integration. Assuming g(t) decays monotonically for large t, the truncation error is an alternating series due to the oscillatory integrand. Then it is possible to choose a minimum T to limit truncation error, since replacement of an alternating series by its n'th partial sum causes an error less than the (n+1)'th contribution to the sum. To this end, take T at a zero-crossing of the oscillating integrand.

The error of a truncated integral, or resolution error, is assessed via error terms from Figure 31. For the specific integrand studied, these are proportional to powers of (Tx/N). Therefore, as higher order methods are used, N is chosen carefully in relation to x and T (the Nyquist sampling rate is one guide). Another way is to use a Rhomberg-type integration, doubling the partition number (each step reusing old computations) until convergence is met. A single call to FFT gives values for the next iteration in Rhomberg's method simultaneously for all sample points $\{x_k\}$.

As a relevant example suppose the Sommerfeld-type integral

$$I(x,y,g) = \int \frac{\exp(jxt)\exp(-p|y|)dt}{2p}$$

where $p^2=t^2+g^2$, is needed at 2M evenly-spaced values x_k in [0,2W]. This example is prompted by application of the point-matching Galerkin's moment method to a microstrip problem: viz., evaluation of the 2-d principal Green's function. Let $T=(2\pi M)L$, where L is an integer large enough for good approximation. Taking the real part of the integral changes the lower limit to zero. By its definition, $x_k=2\pi k/T=k/LM$; $k=0,1,2,\ldots,N-1$. Choose N for desired resolution, and recover every L'th evaluation by the FFT.

Results from this technique are identical to those obtained by other methods (e.g. adaptive Simpson's rule); moreover, the FFT/Simpson's rule method is much faster since a single FFT call returns a needed sequence of integrals for $\{x_k\}$.

Some algorithms already using the FFT might benefit from this slight modification. It also holds promise for evaluation of Sommerfeld-type integrals.

APPENDIX B

APPENDIX B

SURFACE-WAVE CONTRIBUTIONS TO REFLECTED HERTZ POTENTIAL

Integral representations of reflected Green's dyad components, in the axial transform domain, take the form

$$g_{ri} = \int [W_i(L)/4\pi p_c]\exp[ju_x(x-x')]\exp[-p_c(y+y')]du_x$$

where $W_i(L)$ is a generic weighting factor. Note $\mathrm{Re}\{p_c\}>0$ is needed for waves decaying in the cover ($y>0$). Since W_i and p_c are even functions of u_x, the integration interval is halved by symmetry; an integration exclusively over $\mathrm{Re}\{u_x\}>0$ implicates only right-half u_x plane poles.

Rational function $W_i(L)$ carries TE and/or TM surface-wave poles; i.e., $W_i(L)=A_i(L)/Z_i(L)$ where $Z_i(L)=0$ are characteristic equations for even TM or odd TE modes of the symmetric-slab background. Let $L=L_b$ be surface-wave eigenvalues, i.e., solutions of $Z_i(L)=0$. Then $L^2=u_x^2+u_z^2$ locates corresponding u_x-plane poles, where u_z is the propagation eigenvalue leading to nontrivial solutions of the homogeneous EFIE. It is desired to have u_x as an analytic function of L_b and u_z. Since $u_x^2=L^2-u_z^2=-(u_z^2-L^2)$, $u_x=\pm j[(u_z-L)(u_z+L)]^{1/2}$. As only RHP poles are implicated, a criterion for choice of proper branch cut and algebraic sign is $\mathrm{Re}\{u_{xb}\}=0$. This means $|\arg(u_x)|<90^o$, or $|\arg(u_x^2)|<180^o$, defining a u_x plane region for u_x^2 bounded by the negative real axis.

It is necessary to approach the lossless case from a low-loss limit standpoint; wavenumbers (and related quantities such as L_b) are then complex:

$$u_{xb}^2 = L_b^2 - u_z^2 = (L_{br}^2 - L_{bi}^2 - u_{zr}^2 + u_{zi}^2) + 2j(L_{br}L_{bi} - u_{zr}u_{zi})$$

The criteria to meet are

$$\mathrm{Im}\{u_{xb}^2\} = 2(L_{br}L_{bi} - u_{zr}u_{zi}) = 0$$

$$\mathrm{Re}\{u_{xb}^2\} = (L_{br}^2 - L_{bi}^2 - u_{zr}^2 + u_{zi}^2) < 0$$

The first is the hyperbolic branch cut $u_{zi} = L_{br}L_{bi}/u_{zr}$. The second indicates proper hyperbola branches as those asymptotic to the real axis. Define $(u_z - L_b) = r^+ \exp(ja^+)$ and $(u_z + L_b) = r^- \exp(ja^-)$ as u_z-plane phasors directed from $\pm L_b$, respectively, to u_z. See Figure 32. Then $u_x = \pm j(r^+ r^-)\exp[j(a^+ + a^-)/2]$. Since L_{bi} is small in the parameter regime of interest, take $|u_{zi}|$ small with u_{zr} near L_{br}. So a^- is practically 0^0, as is seen graphically, while $-360^0 < a^+ < 0^0$. Therefore $-180^0 < [(a^+ + a^-)/2] < 0^0$, and the plus sign is finally chosen to keep $\mathrm{Re}\{u_{xb}\} > 0$.

Analytical pole contributions to an otherwise numerical integration are of the form

$$D = \lim_{d \to 0} \int_e^f [f_i / Z_i(L)] du_x$$

where $f = du_{xbr} + d$ and $e = u_{xbr} - d$. By Taylor series expansion, $Z_i(L)$ near

the pole is approximately $Z_i(L)=Z_i(L_b)+(u_x-u_{xb})Z_i'(u_{xb})$, where the first term vanishes by definition. Assuming the rest of the integrand is continuous at u_{xb},

$$D = [f_i(u_{xb})/Z_i'(u_{xb})] \lim_{d->0} \int_e^f du_x/(u_x-u_{xb})$$

But

$$\int_e^f du_x/(u_x-u_{xb}) = \int_e^f du_x/[(u_x-u_{xbr})-ju_{xbi}]$$

$$= \ln\{\exp[j[\pm\pi - 2\tan^{-1}(u_{xbi}/d)]]\}$$

$$= j[\pm\pi - 2\tan^{-1}(u_{xbi}/d)]$$

where $|u_{xbi}|$ is understood to be small. Proper choice of algebraic sign in the last expression depends on the sign of u_{xbi}, and precludes crossing the branch cut of the ln function (negative real axis). The argument of the bracketed quantity must fall between -180^o and 180^o. For $u_{xbi}<0$, choose the plus sign; for $u_{xbi}>0$, choose the minus sign. Finally, compute the pole contribution from the preceding formulas.

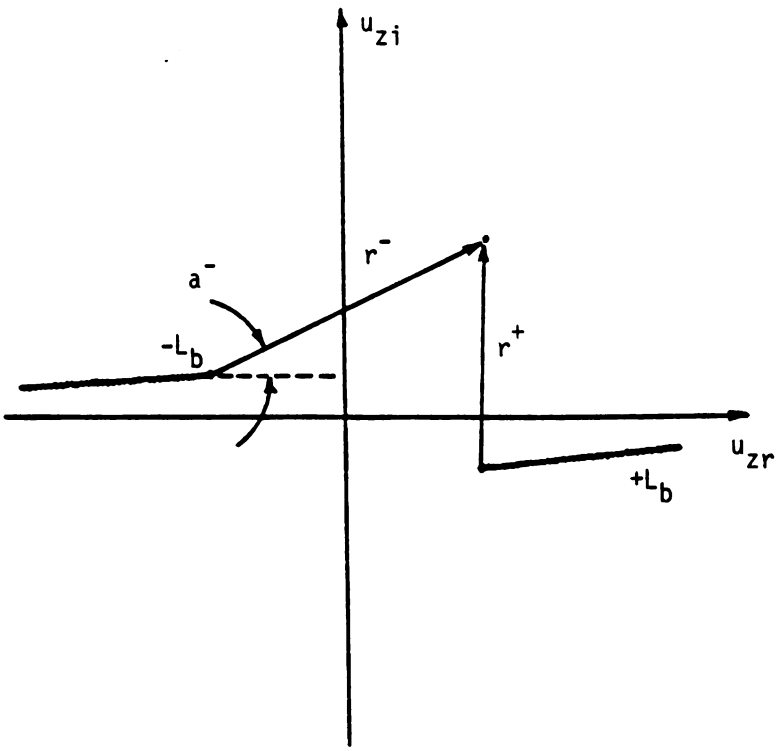

Figure 32. Complex u_z plane phasors.

BIBLIOGRAPHY

BIBLIOGRAPHY

1. T.M. Hyltin, "Microstrip transmission on semiconductor dielectrics," IEEE Trans. Microwave Theory Tech., vol. MTT-13, pp. 777-781, Nov. 1965.

2. Y.T. Lo, D. Solomon, and W.F. Richards, "Theory and experiment on microstrip antennas," IEEE Trans. Antennas Propagat., vol. AP-27, pp. 137-146, 1979.

3. E.J. Denlinger, "A frequency dependent solution for microstrip transmission lines," IEEE Trans. Microwave Theory Tech., vol. MTT-19, pp. 30-39, January 1971.

4. T.T. Wu, "Theory of the microstrip," J. Appl. Phys., vol. 28, pp. 299-302, March 1957.

5. E. Yamashita and R. Mittra, "Variational method for the analysis of microstrip line," IEEE Trans. Microwave Theory Tech., vol. MTT-16, pp. 251-256, April 1968.

6. R.W. Jackson and D.M. Pozar, "Full-wave analysis of microstrip open-end and gap discontinuities," IEEE Trans. Microwave Theory Tech., vol. MTT-33, pp. 1036-1042, October 1985.

7. D.M. Pozar, "Input impedance and mutual coupling of rectangular microstrip antennas," IEEE Trans. Antennas Propagat., vol. AP-30, pp. 1191-1196, November 1982.

8. N.K. Uzunoglu, N.G. Alexopoulos, and J.G. Fikioris, "Radiation properties of microstrip dipoles," IEEE Trans. Antennas Propagat., vol. AP-27, pp. 853-858, November 1979.

9. I.E. Rana and N.G. Alexopoulos, "Current distribution and input impedance of printed dipoles," IEEE Trans. Antennas Propagat., vol. AP-29, pp. 99-105, January 1981.

10. P.B. Katehi and N.G. Alexopoulos, "On the modeling of electromagnetically coupled microstrip antennas - the printed strip dipole," IEEE Trans. Antennas Propagat., vol. AP-32, pp. 1179-1186, November 1984.

11. J.S. Bagby and D.P. Nyquist, "Dyadic Green's functions for integrated electronic and optical circuits," IEEE Trans. Microwave Theory Tech., vol. MTT-35, pp. 206-210, Feb. 1987.

12. S. Ramo, J.R. Whinnery, and T. Van Duzer, Fields and Waves in Communication Electronics, New York: John Wiley and Sons, 1965.

13. R.E. Collin, Field Theory of Guided Waves, New York: McGraw-Hill, 1960.

14. W.K.H. Panofsky and M. Phillips, Classical Electricity and Magnetism, Reading: Addison-Wesley, 1962.

15. A. Sommerfeld, Partial Differential Equations in Physics. New York: Academic Press, 1964.

16. W.R. LePage, Complex Variables and the Laplace Transform for Engineers, New York: Dover Publications, 1961.

17. R.F. Harrington, Field Computation by Moment Methods, New York: The Macmillan Co., 1968.

18. Y. Rahmat-Samii, R. Mittra, and P. Parhami, "Evaluation of Sommerfeld integrals for lossy half-space problems," Electromagnetics, vol. 1, no. 1, pp. 1-28, 1981.

19. K. Araki and T. Itoh, "Hankel transform domain analysis of open circular microstrip radiating structures," IEEE Trans. Antennas Propagat., vol. AP-29, pp. 84-89, 1981.

20. T. Itoh and R. Mittra, "Spectral-domain Approach for calculating the dispersion characteristics of microstrip lines," IEEE Trans. Microwave Theory Tech., pp. 496-499, July 1973.

21. J. Bagby and D. Nyquist, "Radiative and surface wave losses in microstrip transmission lines," Digest of National Radio Science Meeting, National Research Council, January 1987.

22. C.D. Taylor and E.A. Aronson, "An iterative solution of Fredholm integral equations of the first kind," IEEE Trans. Antennas Propagat., pp. 695-696, September 1967.

23. V.K. Tripathi, "A dispersion model for coupled microstrip," IEEE Trans. Microwave Theory Tech., vol. MTT-34, pp. 66-71, January 1986.

24. W.J. Getsinger, "Dispersion of parallel-coupled microstrip," IEEE Trans. Microwave Theory Tech., vol. MTT-21, pp. 144-145, March 1973.

25. J. Bagby, Integral Equation Description of Integrated Dielectric Waveguides, Ph.d. dissertation, Michigan State University, 1984.

26. W.A. Johnson and D.G. Dudley, "Real axis integration of Sommerfeld integrals: source and observation points in air," Radio Science, vol. 18, no. 2, pp. 175-186, March-April 1983.

27. E.O. Brigham, The Fast Fourier Transform, Englewood Cliffs: Prentice-Hall, 1974.

28. A. Papoulis, Signal Analysis, New York: McGraw-Hill, 1977.

29. J.W. Cooley and J.W. Tuckey, "An algorithm for machine calculation of complex Fourier series," Math. Computation, vol. 19, pp. 297-301, April 1965.

30. S.D. Conte and C. de Boor, Elementary Numerical Analysis, 3rd Edition., New York: McGraw-Hill, 1980.

31. M. Abramowitz and I. Stegun, Handbook of Mathematical Functions, New York: Dover Publications, 1972.

32. N. Marcuvitz, "On field representations in terms of leaky modes or eigenmodes," Electromagnetic Wave Theory Symp., pp. 192-194.

33. C.T. Tai, "The effect of a grounded slab on the radiation from a line source," Journal Appl. Phy., vol. 22, pp. 405-414, April 1951.